Khaled Syfullah Fuad

Grid-voltage Synchronization Algorithms Based on Phase-locked Loop and Frequency-locked Loop for Power Converters

School of Electrical Engineering

Thesis submitted for examination for the degree of Master of Science in Technology.

Espoo May 21, 2014

Thesis supervisor:

Prof. Marko Hinkkanen

Aalto University
School of Electrical
Engineering

AALTO UNIVERSITY
SCHOOL OF ELECTRICAL ENGINEERING

ABSTRACT OF THE
MASTER'S THESIS

Author: Khaled Syfullah Fuad

Title: Grid-voltage Synchronization Algorithms Based on Phase-locked Loop and Frequency-locked Loop for Power Converters

Date: May 21, 2014 Language: English Number of pages:10+45

Department of Electrical Engineering and Automation

Professorship: Industrial Electronics and Electrical Drives Code: S-81

Supervisor and instructor: Prof. Marko Hinkkanen

The purpose of this thesis is to study and find the appropriate grid-voltage synchronization method for grid-connected converters under different kinds of faults like phase unbalancing, harmonics, offset and voltage sags. The main purpose of grid-synchronization algorithms is to estimate the positive- and negative-sequence components of the utility voltage under unbalanced and distorted condition. The existing most advanced phase-locked loop (PLL) and frequency-locked loop (FLL) methods are well known method for grid-synchronization. The fundamental variable estimated by the PLL is the grid-phase angle, whereas the grid frequency is the one for the FLL. The most extended technique used for grid synchronization in three-phase three wire system is a synchronous reference frame PLL (SRF-PLL). The SRF-PLL works accurately during balanced condition, but cannot estimate voltage components during unbalanced condition. The Decoupled Double Synchronous Reference Frame PLL (DDSRF-PLL) is might be a substantiation solution for the estimation of the sequence components of the utility voltage under unbalanced condition. Another method based on the FLL, a double second-order generalized integrator FLL (DSOGI-FLL) has also the ability to detect the positive- and negative-sequence components of the utility voltage under unbalanced condition. DDSRF-PLL and DSOGI-FLL algorithms are tested under different kinds of faults and compared with each other. The results show that their performance under harmonic-distorted condition is not really acceptable. A new algorithm based on SRF-PLL, decoupled multiple synchronous reference frame PLL (DMSRF-PLL) might be a better solution for accurate detection of the positive- and negative-sequence voltage components under unbalanced and harmonic distortion condition.

Keywords: decoupling network, frequency-locked loop, grid-connected converter, phase-locked loop, second order generalized integrator

Preface

The content and result of this thesis are the outcome of a study where several persons have contributed with guidance, knowledge, experience and ideas - not to mention their valuable time.

First I would like to express my gratitude to professor Marko Hinkkanen, for careful examination of the thesis. During the study, he has provided me with much useful advice that has contributed to the outcome.

I thank Jussi Koppinen and specially to Jarno Kukkola for their support and valuable suggestions, which has helped me to ride through lot of obstacles during my thesis.

I have gained lots of new knowledge during my thesis, which not only has increased my understanding in this field of study but also encouraged me to do research as a professional in near future.

At last, I want to mention that I am grateful to my God for being so merciful and giving me the opportunity to complete my master thesis.

Otaniemi, 21.05.2014

Khaled Syfullah Fuad

Contents

List of Figures

Symbols and abbreviations

Symbols

$\mathbf{i}$	current space vector
$\mathbf{i}_{abc}$	three-phase current
i_a, i_b, i_c	phase currents of a, b, c respectively
$\mathbf{i}^+, \mathbf{i}^-$	positive- and negative-sequence current space vector
k_p	proportional gain
k_i	integral gain
p	active power
P	average value of the active power
$\tilde{p}$	oscillatory value of the active power
q	reactive power
Q	average value of the reactive power
$\tilde{q}$	oscillatory value of the reactive power
u	input voltage
$\hat{u}$	estimated value of u
$\mathbf{u}_{abc}$	three-phase voltage
u_a, u_b, u_c	phase voltages of a, b, c respectively
U_a, U_b, U_c	peak value of phase voltages a, b, c respectively
$U_m/U_+, U_n/U_-$	peak value of positive- and negative-sequence voltages respectively
$\mathbf{u}^+_{abc}, \mathbf{u}^-_{abc}, \mathbf{u}^0_{abc}$	positive- , negative- and zero-sequence voltages of three-phase voltage
$\mathbf{u}^s$	space vector in stationary coordinates
$\mathbf{u}^s_+, \mathbf{u}^s_-$	positive- and negative-sequence voltage vectors in stationary coordinates
u_α, u_β	α and β components of space vector in stationary coordinates respectively
$\mathbf{u}$	space vector in synchronous coordinates
$\mathbf{u}^+, \mathbf{u}^-$	positive- and negative-sequence voltage vectors in synchronous coordinates
$\mathbf{u}^T$	transpose of matrices $\mathbf{u}$
u_d, u_q	d and q components of space vector in synchronous coordinates respectively
$\hat{u}_d, \hat{u}_q$	estimated values of u_d and u_q respectively
$u^n_d/u^+_d/u^{+1}_d$	positive-sequence voltage vector of d component
$\hat{u}^n_d/\hat{u}^{+1}_d$	estimated positive-sequence voltage vector of d component
$\overline{u}^n_d/\overline{u}^{+1}_d$	dc value of positive-sequence voltage vector of d component
$u^m_d/u^-_d/u^{-1}_d$	negative-sequence voltage vector of d component
$\hat{u}^m_d/\hat{u}^{-1}_d$	estimated negative-sequence voltage vector of d component
$\overline{u}^m_d/\overline{u}^{-1}_d$	dc value of negative-sequence voltage vector of d component
$u^n_q/u^+_q/u^{+1}_q$	positive-sequence voltage vector of q component
$\hat{u}^n_q/\hat{u}^{+1}_q$	estimated positive-sequence voltage vector of q component
$\overline{u}^n_q/\overline{u}^{+1}_d$	dc value of positive-sequence voltage vector of q component
$u^m_q/u^-_q/u^{-1}_q$	negative-sequence voltage vector of q component
$\hat{u}^m_q/\hat{u}^{-1}_q$	estimated negative-sequence voltage vector of q component
$\overline{u}^m_q/\overline{u}^{-1}_d$	dc value of negative-sequence voltage vector of q component

Greek Letters

θ	phase angle of three phase voltage
$\hat{\theta}$	estimated phase angle of three phase voltage
ϕ_a, ϕ_b, ϕ_c	phase angles of a, b, c respectively
ϕ^m/ϕ^{+1}	positive-sequence phase angle of three-phase voltage
ϕ^m/ϕ^{-1}	negative-sequence phase angle of three-phase voltage
ω	fundamental frequency of three-phase voltage
$\hat{\omega}$	estimated frequency of three-phase voltage
ω_f	cut-off frequency of the LPF
ω_{PLL}	control loop frequency
ξ	damping constant
ξ_{PLL}	damping constant of PLL
ε_u	synchronization error signal
ε_f	frequency error variable

Abbreviations

AF	adaptive filter
DPGS	distributed power generation system
DVR	dynamic voltage restorers
DSRF	double Synchronous Reference Frame
DDSRF	decoupled double synchronous reference frame
DSOGI	double second-order generalized integrator
DMSRF	decoupled multiple synchronous reference frame
FRT	fault ride through
FLL	frequency-locked loop
FLL	frequency-locked loop
ISC	instantaneous symmetrical components
GI	generalized Integrator
GCRs	grid connection requirements
GSC	grid side converter
LPF	low pass filter
MSHDC	multi-sequence/harmonic decoupling cell
MSOGI	multiple second-order generalized integrator
PWM	pulse-width modulation
PV	photovoltaic
PLL	phase-locked loop
QSG	quadrature signal generator
RES	renewable energy source
SDRF	synchronous double reference frame
SRF	synchronous reference frame
SOGI	second-order generalized integrator
STATCOM	static synchronous compensator
SVF	space vector filters
VCO	voltage controlled oscillator
WLSE	weighted least-square estimation algorithm
WT	wind turbine

1 Introduction

1.1 Background

An electric grid is an interconnected network for delivering electricity from suppliers to consumers. Electrical grids are affected by various occurrences like continuous connection and disconnection of loads, harmonics, faults caused by nature or equipment failure. Penetration of distributed power generation systems (DPGS) based on renewable energy sources (RES) in recent year have increased significantly. Grid connection requirements (GCRs) state that DPGS should ride through grid disturbance without tripping as successfully as the conventional power plants they replace. The widespread use of power electronics systems will result even better performance than the conventional power plants. This requires the improvement of control and design of power converters for ride through different kinds of faults. The control scheme of the grid-side converter (GSC) mostly depends on two cascade loops. One is an internal current loop, which regulates the grid current and another one is external voltage loop, which controls the dc-link voltage. The control of the GSC is based on a dc-link voltage loop and it is designed for balancing the power flow in the system [1].

RES require accurate and appropriate performance not only under normal grid operation but also under abnormal and faulty grid conditions according to the modern grid codes. The appropriate operation of the interconnected RES is achieved by controlling the GSC properly. The proper control of the GSC can be ensured by accurate synchronization. So the grid synchronization algorithms for fast and accurate detection of the grid voltage parameters are of great importance in the control of grid-connected power converters for implement stable control strategies under generic grid conditions.

Three-phase power converters used in wind turbine (WT) and photovoltaic (PV) systems generally inject positive sequence currents at the fundamental frequency into the grid and only intentionally inject negative-sequence and harmonic currents in unusual cases, i.e. either avoiding power oscillations to protect the power converter or injecting unbalanced reactive currents to compensate the unbalanced grid voltage at the point of common coupling (PCC) [1]. So the correct detection of the positive- and negative-sequence component at the fundamental frequency of the three-phase grid voltage can be considered as the main task of the synchronization system of a grid-connected three-phase power converter.

As per the requirement, the grid-voltage synchronization by using phase-locked loop (PLL) is became an conventional way of grid-synchronization. There is an another method based won frequency-locked loop (FLL) might be an alternative choice for grid-synchronization. The fundamental variable estimated by the PLL is the grid-phase angle, whereas the grid frequency is the one for the FLL.

The purpose of the synchronization algorithm is to extract the positive- and negative sequence voltage, phase angle and the frequency of the grid voltage [3]. Most of the faults create unbalanced voltages and, as a result, fast and accurate detection of the positive and negative sequence components of the grid voltage is important in order to control energy transfer and keep generation up according to GCRs.

The energy transfer and power flows between the ac mains and a grid-connected power converter mostly depend on the angle ϕ between them. The control of grid-connected power converter requires an on-line tracking of the ac mains voltage phase angle θ in order to calculate the suitable firing signals. Phase locked-loop (PLL) system and frequency-locked loop (FLL) be designed to detect the unbalance condition in the control structure by extract the phase angle θ and frequency ω of the grid voltages, respectively. Three-phase synchronous reference frame PLL (SRF-PLL) is broadly use for detecting the positive-sequence component of the voltage. But it cannot estimate the voltage components during unbalanced condition due to the appearance of negative-sequence voltage in the unbalanced system.

1.2 Structure of the Thesis

In forthcoming sections in this thesis, two most advanced grid-synchronization algorithms decoupled double synchronous reference frame PLL (DDSRF-PLL) and second-order generalized integrator FLL (SOGI-FLL) for detecting the positive- and negative-sequence components at the fundamental frequency of the three-phase grid voltage are studied and modelled. In section 8, their performance under different fault conditions are tested and evaluated. The results show that both DDSRF-PLL and SOGI-FLL can perfectly detect the positive- and negative-sequence voltage components under unbalanced condition. But both DDSRF-PLL and SOGI-FLL cannot perfectly detect the positive- and negative-sequence voltage components under unbalanced and harmonic distortion condition.

Finally in section 9, conclusion, as a future work of this thesis, a new algorithm based on SRF-PLL, decoupled multiple synchronous reference frame PLL (DMSRF-PLL) has been proposed. DMSRF-PLL will have the ability of accurate detection of the positive- and negative-sequence voltage components under unbalanced and harmonic distortion condition.

2 Three-phase Balanced and Unbalanced System

The three-phase utility voltage abc can be written as [27],

$$\mathbf{u}_{abc}(t) = \begin{bmatrix} u_a(t) \\ u_b(t) \\ u_c(t) \end{bmatrix} = \begin{bmatrix} U_a \cos(\omega t + \phi_a) \\ U_b \cos(\omega t - \frac{2\pi}{3} + \phi_b) \\ U_c \cos(\omega t + \frac{2\pi}{3} + \phi_c) \end{bmatrix} \tag{1}$$

where U_a, U_b and U_c are the peak value of $u_a(t)$, $u_b(t)$ and $u_c(t)$ phase voltages, respectively. During normal operation $\hat{U}_a \approx \hat{U}_b \approx \hat{U}_c$ and ϕ_a, ϕ_b and ϕ_c are small.

2.1 Sequences

Normal situation of a three-phase system with equal peak values in all three phases, and absolutely 120° phase distribution. This is known as a symmetric system. When phase b lags behind phase a by 120°, it is known as positive sequence:

$$\mathbf{u}_{abc}(t) = \begin{bmatrix} u_a(t) \\ u_b(t) \\ u_c(t) \end{bmatrix} = \begin{bmatrix} U_a \cos(\omega t) \\ U_b \cos(\omega t - \frac{2\pi}{3}) \\ U_c \cos(\omega t + \frac{2\pi}{3}) \end{bmatrix} \tag{2}$$

But if this order is not followed, and phase b lags behind phase a by 240^o, the system has negative sequence:

$$\mathbf{u}_{abc}(t) = \begin{bmatrix} u_a(t) \\ u_b(t) \\ u_c(t) \end{bmatrix} = \begin{bmatrix} U_a \cos(\omega t) \\ U_b \cos(\omega t + \frac{2\pi}{3}) \\ U_c \cos(\omega t - \frac{2\pi}{3}) \end{bmatrix} \tag{3}$$

The un-symmetric three-phase system in (1) can be decomposed in a positive sequence, a negative sequence and a zero sequence,

$$\mathbf{u}_{abc}(t) = \begin{bmatrix} u_a(t) \\ u_b(t) \\ u_c(t) \end{bmatrix} = \underbrace{\begin{bmatrix} U_+ \cos(\omega t + \phi^{+1}) \\ U_+ \cos(\omega t - \frac{2\pi}{3} + \phi^{+1}) \\ U_+ \cos(\omega t + \frac{2\pi}{3} + \phi^{+1}) \end{bmatrix}}_{\mathbf{u}^+_{abc}} + \underbrace{\begin{bmatrix} U_- \cos(\omega t + \phi^{-1}) \\ U_- \cos(\omega t + \frac{2\pi}{3} + \phi^{-1}) \\ U_- \cos(\omega t - \frac{2\pi}{3} + \phi^{-1}) \end{bmatrix}}_{\mathbf{u}^-_{abc}} + \underbrace{\begin{bmatrix} u_0(t) \\ u_0(t) \\ u_0(t) \end{bmatrix}}_{\mathbf{u}^0_{abc}} \tag{4}$$

where U_+ and U_- are the peak value of the positive and negative sequence components and $\mathbf{u}^+_{abc}, \mathbf{u}^-_{abc}, \mathbf{u}^0_{abc}$ are positive- , negative- and zero-sequence voltages of three-phase voltage. Here $u_0(t)$ is zero sequence component and expressed as,

$$u_0(t) = \frac{u_a(t) + u_b(t) + u_c(t)}{3} \tag{5}$$

2.2 Space Vector Transformations

The Clarke Transformation is used to express the utility voltage into the stationary reference frame $\alpha\beta$. For symbolic notation, the space vector in stationary coordinates, is denoted by, superscript s of the vector itself and its components are denoted

by, subscripts α and β respectively [9]. Then the utility voltage vector is,

$$\mathbf{u}^s = \begin{bmatrix} u_\alpha \\ u_\beta \end{bmatrix} = \underbrace{\frac{2}{3}\begin{bmatrix} 1 & -\frac{1}{2} & -\frac{1}{2} \\ 0 & \frac{\sqrt{3}}{2} & \frac{\sqrt{3}}{2} \end{bmatrix}}_{[T_{\alpha\beta}]} \begin{bmatrix} u_a \\ u_b \\ u_c \end{bmatrix} \tag{6}$$

(where we from here on drop the time argument "(t)," for simplicity). It is seen from the (6) that the zero sequence of abc is eliminated. Basically, most of the three phase and three wire systems do not have a physical neutral wire connection. The advantage of it is, that, phase to phase voltage can be utilized for reducing the number of voltage sensors and also the components in transformation matrix. So the (6) can be rewritten as [7],

$$\mathbf{u}^s = \begin{bmatrix} u_\alpha \\ u_\beta \end{bmatrix} = [T_{\alpha\beta}] \begin{bmatrix} u_a - u_c \\ u_b - u_c \\ u_c - u_c = 0 \end{bmatrix} \tag{7}$$

These can be transformed into synchronous dq reference frame through Park's transformation. For symbolic notation, the space vector in synchronous coordinates, is denoted by boldface of the vector itself and its components are denoted by, subscripts d and q, respectively.

$$\mathbf{u} = \begin{bmatrix} u_d \\ u_q \end{bmatrix} = \begin{bmatrix} \cos\theta & \sin\theta \\ -\sin\theta & \cos\theta \end{bmatrix} \begin{bmatrix} u_\alpha \\ u_\beta \end{bmatrix} \tag{8}$$

where $\theta = \int \omega dt$, in steady state and θ and ω are the original phase angle and frequency of the input voltage vector. Now the voltage vector $\mathbf{u}^s$ can be written for positive and negative sequence components as,

$$\mathbf{u}^s = \mathbf{u}^s_+ + \mathbf{u}^s_- = U_+ \begin{bmatrix} \cos(\omega t) \\ \sin(\omega t) \end{bmatrix} + U_- \begin{bmatrix} \cos(-\omega t + \phi^{-1}) \\ \sin(-\omega t + \phi^{-1}) \end{bmatrix} \tag{9}$$

where $\mathbf{u}^s$ consist of two sub-vetors; $\mathbf{u}^s_+$, rotating with a positive angular frequency ω and $\mathbf{u}^s_-$, rotating with a negative angular frequency $-\omega$.

2.3 Voltage Sags

A voltage sag, also known as a voltage dip, is a sudden reduction of the grid voltage, usually between 10 to 90% of the rated value, for a period lasting from half a cycle to a few seconds. Different type of grid fault and depending on the transformer connections along the power lines, voltage sags can be characterized in separate. A detailed explanation about this topic can be found in [31]-[32]. The voltage sags classification are given below:

1. Sag type A. Three-phase fault and three-phase-to-ground fault.

2. Sag type B. Single-phase-to-ground fault.

3. Sag type C. Phase-to-phase fault.

4. Sag type E. Two-phase-to-ground fault.

The type of sag experienced by a system connected to a given AC bus not only depend on the number of phases affected by the grid fault but it is also depend on the transformers location in between the AC bus and the fault point. The amplitude and phase angle of the unbalanced voltage resulting from a given grid fault will change, when propagated through regular three-phase transformer used in the network, which will give rise to new types of voltage sags, different to the ones has classified earlier. After this, due to the propagation of voltage sags, the new type of voltage sags are classified below. Moreover, the zero-sequence component, normally present in phase-to-ground faults, will be removed.

1. Sag type D. Propagation of sag type C.

2. Sag type F. Propagation of sag type E.

3. Sag type G. Propagation of sag type F.

As an example, a sag type C is given below:

$$\begin{bmatrix} U_a \\ U_b \\ U_c \end{bmatrix} = \begin{bmatrix} 1 \\ -\frac{1}{2} - \frac{\sqrt{3}}{2}D \\ -\frac{1}{2} + \frac{\sqrt{3}}{2}D \end{bmatrix} U_{pf}$$
$$\begin{bmatrix} U_+ \\ U_- \\ U_0 \end{bmatrix} = \begin{bmatrix} \frac{1}{2}(1+D) \\ \frac{1}{2}(1-D) \\ 0 \end{bmatrix} U_{pf} \tag{10}$$

where U_{pf} represents the pre-fault voltage vector of one of the phase in a three-phase balanced system and D is the characteristic phase angle jump of the voltage sag.

3 Basic control of Grid-connected Power Converter

Grid-connected power converters in a distributed generation system are connected in electrical network system, which can be affected by various grid faults because of many factors. The control of these power converters under abnormal condition should guarantee that the protection of the converter would not trip but also need to support the grid voltage under these conditions. Grid faults mostly give rise of unbalanced grid voltages at the PCC and as a result the currents injected into the grid get non-sinusoidal and lose their balanced operation. As a result the combination of these unbalanced grid voltages and such currents give rise to uncontrolled oscillations in the active and reactive power delivered to the network. The accurate operation of the power converter under these conditions is one of the main control task [1].

Grid-voltage synchronization algorithm has the ability to detect the positive and negative sequence components of unbalanced utility voltage during different kind of faults. These different sequences of grid voltage are used to calculate the current reference $\mathbf{i}_{\text{ref}}$, which plays an important role on the delivered power quality during the fault [22]. As we can see from Fig. 1, the grid synchronization block performs the estimation of the magnitude, frequency and phase angle of the positive- and the negative-sequence components of the grid voltage $\mathbf{u}^{+}_{abc}$, $\mathbf{u}^{-}_{abc}$, ω, and θ, respectively. After that, these estimated values are used at the current controller block, which settles finally the voltage waveform $\mathbf{u}_{\text{ref}}$ to be modulated as well as at the reference generator, responsible of determining the current reference to be tracked [9]. The last block power converter on the left hand side, will vary accordingly as an active filter, a static synchronous compensator (STATCOM), or a power processor, depending on the power generation plant. The values of the synchronization loop could affect the generation of the reference currents, the dynamics of the current controller, and also the calculation of the *dq* component of the grid voltage and injected currents. These phenomenons sum up that a faster and accurate performance of the synchronization loop has great importance for the control of the GSC [23].

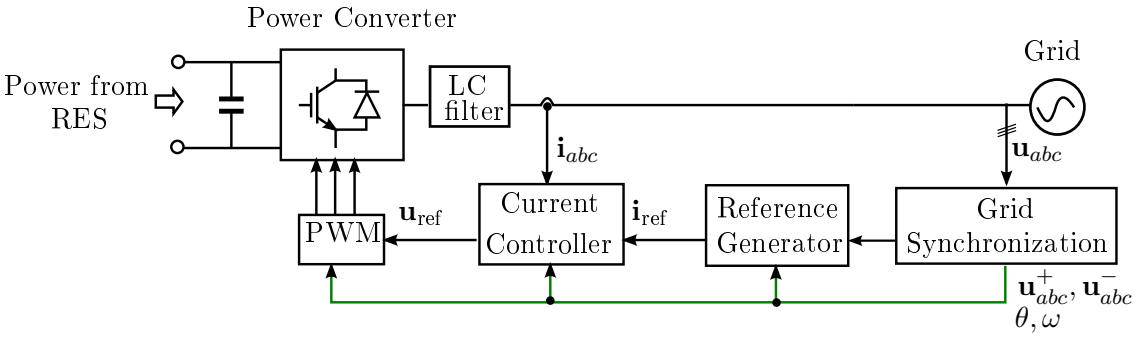

Figure 1: Generic grid synchronization application for the control of a grid connected three-phase power converter.

3.1 Power Control during Unbalanced Grid Conditions

Under unbalanced conditions, the control of the instantaneous active and reactive power exchanged with the grid requires accurate control strategy. Most importantly, the appearance of the power oscillating terms as a result of the interaction between voltages and currents with different sequences, needs accurate control structure for calculating the current, which needs to be injected into the grid.

Now, the instantaneous active power, p, supplied or drained by a grid-connected three-phase power converter can be written in synchronous coordinates as [1],

$$\begin{aligned} p &= \frac{3}{2}\mathbf{u}^T\mathbf{i} \\ &= \frac{3}{2}(u_d i_d + u_q i_q) \end{aligned} \tag{11}$$

where $\mathbf{u}$ is the voltage vector at the PCC and $\mathbf{i} = \begin{bmatrix} i_d & i_q \end{bmatrix}^T$ is the injected current vector in such a point. The subscript ' T ' indicates transpose of matrices. Now, if we consider the symmetrical components of both voltage and current, (11) can be written as,

$$\begin{aligned} p &= \frac{3}{2}\left[(\mathbf{u}^+)^T + (\mathbf{u}^-)^T\right]\left[\mathbf{i}^+ + \mathbf{i}^-\right] \\ &= \underbrace{\frac{3}{2}\left[(\mathbf{u}^+)^T\mathbf{i}^+ + (\mathbf{u}^-)^T\mathbf{i}^-\right]}_{P} + \underbrace{\frac{3}{2}\left[(\mathbf{u}^+)^T\mathbf{i}^- + (\mathbf{u}^-)^T\mathbf{i}^+\right]}_{\tilde{p}} \end{aligned} \tag{12}$$

where subscripts '+' and '−' denote the positive and negative sequence variables, respectively. In (12), the area over P on the bracket is the average value and second area over $\tilde{p}$ on the bracket is the oscillatory value of the active power, respectively.

Now the instantaneous active power, q, is defined as,

$$\begin{aligned} q &= \frac{3}{2}\mathbf{u}^T\mathbf{J}\mathbf{i} \\ &= \frac{3}{2}(u_q i_d - u_d i_q) \end{aligned} \tag{13}$$

where $\mathbf{J} = \left[\begin{smallmatrix} 0 & -1 \\ 1 & 0 \end{smallmatrix}\right]$ [27]. Now, again we can consider the symmetrical components of both voltage and current for (13),

$$\begin{aligned} q &= \frac{3}{2}\left[(\mathbf{u}^+)^T + (\mathbf{u}^-)^T\right]\left[\mathbf{J}\mathbf{i}^+ + \mathbf{J}\mathbf{i}^-\right] \\ &= \underbrace{\frac{3}{2}\left[(\mathbf{u}^+)^T\mathbf{J}\mathbf{i}^+ + (\mathbf{u}^-)^T\mathbf{J}\mathbf{i}^-\right]}_{Q} + \underbrace{\frac{3}{2}\left[(\mathbf{u}^+)^T\mathbf{J}\mathbf{i}^- + (\mathbf{u}^-)^T\mathbf{J}\mathbf{i}^+\right]}_{\tilde{q}} \end{aligned} \tag{14}$$

In (14), first area over Q on the bracket is the average value and second area over $\tilde{q}$ on the bracket is the oscillatory value of the reactive power, respectively.

3.2 Current Reference Strategies Delivering Active and Reactive Power

As mentioned earlier, new GCRs demand that wind turbines have to ride-through severe operating conditions originated by transient faults. However, it is not specified that how the currents injected by the WT should be during the grid fault [22]. Grid faults can be classified into two type, balanced or unbalanced. In the situation of balanced grid fault, where the operation of the grid converter is similar to the normal grid condition with the only difference that the current in the grid side converter is increasing because of the reduction of the grid voltage amplitude. Secondly, in the situation of unbalanced grid fault, the appearance of negative sequence has affect on the control of grid side converter.

Different strategies can be applied to calculate the current references for a three-phase grid connected converter delivering the same mean value of active and reactive powers to an unbalanced grid. Some strategies which are mentioned in [1], is given below:

1. Instantaneous Active and Reactive Control (IARC). IARC strategy performs well under balanced condition. But the performance of IARC under unbalanced condition is not really acceptable [1].

2. Positive and Negative Sequence Control (PNSC). PNSC strategy performs well under balanced and unbalanced conditions [1].

The study above shows, how important it is to detect the fundamental-frequency positive and negative sequence component of unbalanced utility voltage during grid faults. The information provided by the grid-voltage synchronization method is used to design the current control strategies which lead to different power delivery strategies. So, the accurate detection of the positive- and negative-sequence components of the utility voltage has an important role in controlling the grid-connected power converter during and after the fault [22].

4 Three Phase Synchronous Reference Frame PLL System

The correct detection of the positive-sequence component at the fundamental frequency of the three-phase grid voltage is considered as the main task of the synchronization system of a grid-connected three-phase power converter in balanced condition [1].

The positive-sequence voltage magnitude and the angle are used for the synchronization of the converter output variables, for the transformation of state variables into rotating reference frames, power flow calculation.

Two main approaches are used for detect the positive sequence component of the utility voltage [8]:

1. Assuming the frequency of the utility is a constant and well known magnitude, and is based on instantaneous symmetrical components (ISC), on space vector filters (SVF), or on the recursive weighted least-square estimation algorithm (WLSE).

2. Assuming the frequency of the utility is not constant or insensitive.

The most popular method used for frequency insensitive positive-sequence detection is the three-phase phase locked loop (PLL) based on the synchronous reference frame (SRF-PLL). A SRF-PLL controller is suitable for a balanced system. For an unbalanced system, a second reference frame rotating in the opposite direction is also need to track down the negative sequence component.

4.1 Phase Locked Loop

The PLL is a closed loop system having an internal oscillator which is controlled to keep the time of some external periodical signal by using the feedback loop. A grid-connected power converter should phase lock its internal oscillator to some particular power grid signal for generating amplitude and phase-coherent internal signal which is used by different blocks in the control system. Advanced synchronous control systems based on fast and precise PLLs are applied in grid converters. PLL provides continuous information about the phase angle and the magnitude of the

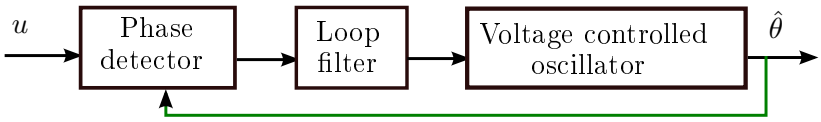

Figure 2: Basic structure of a PLL.

fundamental grid voltage mostly, which helps to implement space vector based controllers and modulators [1].

The basic structure of a PLL is shown in Fig. 2. It has three common blocks [1]:

1. **The Phase Detector**: The average value of its output is zero only when the averaged each cycle of the fundamental components of the input signal u are in phase, means they are synchronized both in phase $\hat{\theta} = \theta$ and frequency $\hat{\omega} = \omega$, where $\hat{\theta}$ and $\hat{\omega}$ are the phase angle and frequency detected by the PLL, respectively.

2. **The Loop Filter**: This block has low pass filter (LPF) characteristics and supply a filtered control signal to the voltage controlled oscillator (VCO) and set the dynamics of the system. Mostly this is a first order LPF or PI controller.

3. **The Voltage Controlled Oscillator (VCO)**: The VCO generates a signal whose frequency varies with respect to a central frequency as a function of the input voltage.

4.2 Basic Structure of Three Phase Synchronous Reference Frame PLL

The proper block diagram of a three-phase PLL is shown in Fig. 3. For achieving the synchronisation between dq reference frames with the $\alpha\beta$ vector, a control loop such as PLL is used use to force $u_q = 0$. The PLL frequency and phase angle can track the utility frequency and phase angle, respectively, by the proper design of the loop filter [4]. Here the loop filter is a proportional-integral (PI) controller, where k_p and k_i are proportional and integral gain, respectively. When the utility voltage is balanced and sinusoidal, the $\alpha\beta$ vector has a constant magnitude equal to the peak of the phase voltage having a constant frequency ω. In steady state, the magnitude of u_d is equal to the peak value of the utility phase voltage and $\hat{\theta} = \theta$. But when the voltage is unbalanced and contains negative sequence and harmonics, the voltage vector magnitude u_d and the $\hat{\theta}$ is not constant due to the 2ω oscillation. This is because of the appearance of the negative-sequence of the voltage [5].

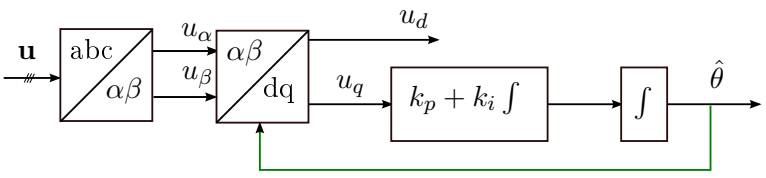

Figure 3: Control diagram of the conventional three-phase synchronous dq frame PLL system.

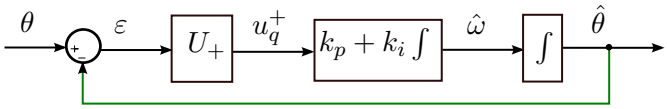

Figure 4: Linearized control loop

The amplitude and angular position of the voltage vector $\mathbf{u}^s$ can be calculated as from (9),

$$|\mathbf{u}^s| = \sqrt{(U_+)^2 + (U_-)^2 + 2U_+U_-\cos(-2\omega t + \phi^{-1})} \tag{15a}$$

$$\theta = \omega t + \tan^{-1}\left(\frac{U_-\sin(-2\omega t + \phi^{-1})}{U_+ + U_-\cos(-2\omega t + \phi^{-1})}\right) \tag{15b}$$

4.3 Selection of the PI controller parameters

From Fig. (3), it can be seen that the feedback variable $\hat{\theta}$ has a linear relation with u_q. From this expression, the linearized control diagram shown in Fig. 4 and this is discussed broadly in [4],[6] and [28]. The transfer functions of the system are,

$$\frac{\hat{\theta}(s)}{\theta(s)} = \frac{2\xi_{\text{PLL}}\omega_{\text{PLL}}s + \omega_{\text{PLL}}^2}{s^2 + 2\xi_{\text{PLL}}\omega_{\text{PLL}}s + \omega_{\text{PLL}}^2} \tag{16}$$

$$\frac{\varepsilon(s)}{\theta(s)} = \frac{s^2}{s^2 + 2\xi\omega_{\text{PLL}}s + \omega_{\text{PLL}}^2} \tag{17}$$

where control loop frequency, $\omega_{\text{PLL}} = \sqrt{U_+k_i}$; damping constant, $\xi_{\text{PLL}} = \frac{k_p}{2}\sqrt{\frac{U_+}{k_i}}$ and from these we can calculate the value for the control loop gains k_p and k_i.

4.4 Performance of SRF-PLL

The SRF-PLL is built in MATLAB Simulink environment and simulated to observe the performance in balanced and unbalanced condition. The balanced condition input voltage is characterized as $U_+ = 100$ V, $U_- = 0$ V, $\phi^{-1} = 0$ and $\omega = 2\pi 50$ rad/s. From Fig. 5(a), we can observe that in balanced condition, the PLL frequency $\hat{\omega}$ and phase angle $\hat{\theta}$ can perfectly track the utility frequency ω and θ, respectively.

For unbalanced condition, the input voltage is characterized as $U_+ = 100$ V, $U_- = 30$ V, $\phi^{-1} = 0$ and $\omega = 2\pi 50$ rad/s and appears after 0.3 s, being the prefault grid voltage equal to $U_{\text{pf}} = 100$ V. The values for the PI controller is $k_p = 44.42$ and $k_i = 9.87 \times 10^4$ is selected according to [9]; which results the value for $\omega_{\text{PLL}} \approx 2\pi 500$ rad/s and $\xi_{\text{PLL}} \approx 1/\sqrt{2}$. With this higher bandwidth, the SRF-PLL almost has $u_q \approx 0$ under unbalanced condition. The oscillation in the estimated values of u_d and $\hat{\theta}$ in Fig. 5(b) shows that these values cannot be correctly determined with this higher bandwidth. This is because of the oscillation term 2ω appears in unbalanced

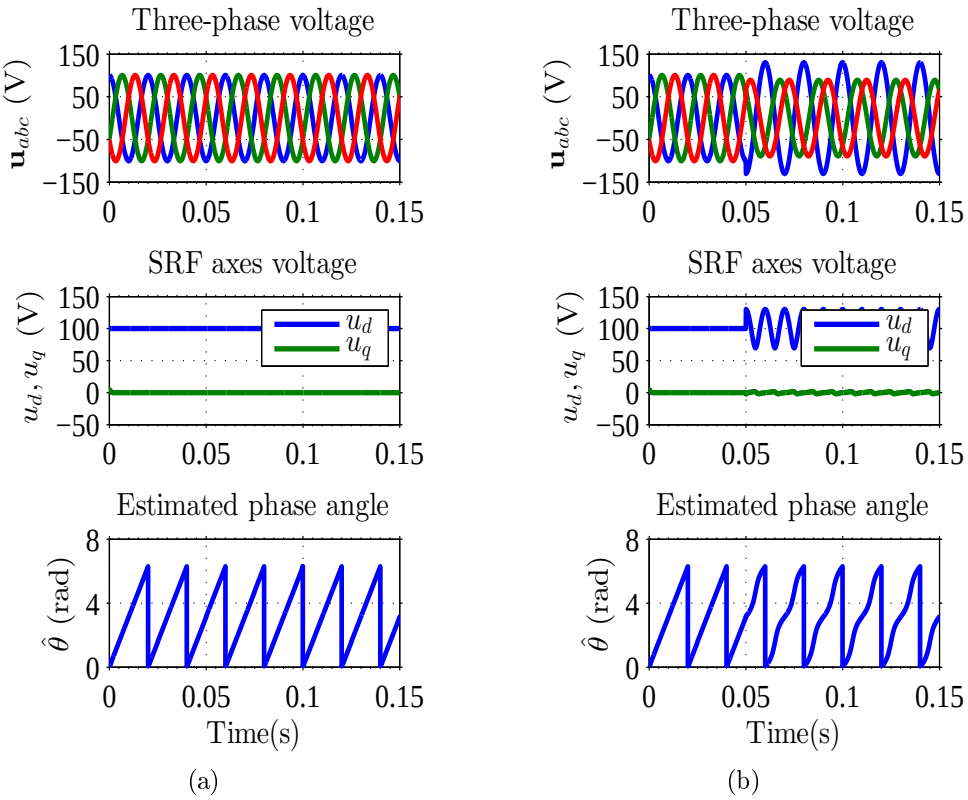

Figure 5: Performance of SRF-PLL under (a) balanced and (b) Unbalanced condition.

condition due to the negative sequence of the voltage, which is shown in (15a) and (15b).

For a better estimation of u_d and $\hat{\theta}$, the control loop bandwidth can be reduced and LPF can be used [9]. But these techniques have limitations; the phase angle and the positive-sequence voltage cannot be accurately detected and the dynamic response of the system will be reduced significantly. But the grid condition requires the accurate detection of the grid parameters and excellent dynamic response like dynamic voltage restorers (DVR) under unbalanced conditions, conventional SRF-PLL technique is not the appropriate solution for the control of power converters.

5 Decoupled Double Synchronous Reference Frame PLL for Power Converter Control

Decoupled double synchronous reference frame PLL (DDSRF-PLL) technique has the ability of fast and accurate detection of the positive-sequence component of an unbalanced voltage vector having both positive- and negative-sequence component, which later expresses on the double synchronous reference frame (DSRF) for detecting the positive-sequence component [8].

5.1 Double Synchronous Reference Frame

In Double synchronous reference frame PLL system, the $\mathbf{u}^s$ in (6) projected on two different rotating reference frames. The first one is dq^+ reference frame rotating with $\hat{\omega}$ frequency is synchronized with $\mathbf{u}^s_+$ and second one is dq^- reference frame rotating with $-\hat{\omega}$ frequency is synchronized with $\mathbf{u}^s_-$ [6]. Fig. 6 shows the synchronous double reference frame (SDRF) and the representation of voltage vectors with the reference axes. The expression $\mathbf{u}^s$ on these reference frames is,

$$\mathbf{u}^+ = \begin{bmatrix} u_d^+ \\ u_q^+ \end{bmatrix} = [T_{dq}^+]\mathbf{u}^s \tag{18a}$$

$$\mathbf{u}^- = \begin{bmatrix} u_d^- \\ u_q^- \end{bmatrix} = [T_{dq}^-]\mathbf{u}^s \tag{18b}$$

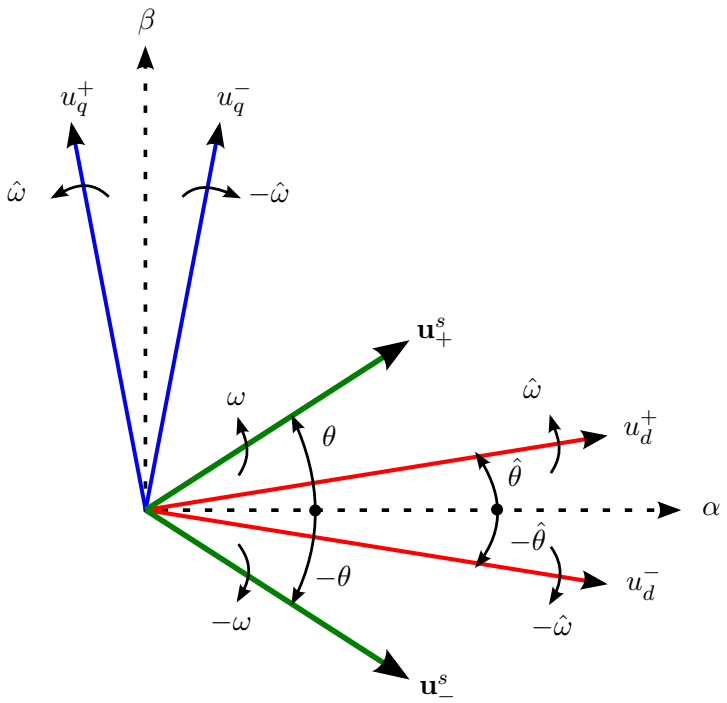

Figure 6: SDRF. Representation of voltage vectors with the reference axes.

where the superscript '+' represent the vectors rotating with a positive angular frequency ω and '$-$' represent the vectors rotating with a negative angular frequency $-\omega$, respectively. The synchronous transformation matrices $[T_{dq}^{+}]$ and $[T_{dq}^{-}]$ are,

$$[T_{dq}^{+}] = \begin{bmatrix} \cos\hat{\theta} & \sin\hat{\theta} \\ -\sin\hat{\theta} & \cos\hat{\theta} \end{bmatrix} \tag{19a}$$

$$[T_{dq}^{-}] = \begin{bmatrix} \cos\hat{\theta} & -\sin\hat{\theta} \\ \sin\hat{\theta} & \cos\hat{\theta} \end{bmatrix} \tag{19b}$$

where $\hat{\theta} = \int \hat{\omega} dt$ holds during transients.

Now from (9), (18a), (18b), (19a) and (19b) we get,

$$u_d^{+} = U_{+}\cos(\omega t - \hat{\theta}) + U_{-}\cos(-\omega t + \phi^{-1} - \hat{\theta}) \tag{20a}$$

$$u_d^{-} = U_{+}\cos(\omega t + \hat{\theta}) + U_{-}\cos(-\omega t + \phi^{-1} + \hat{\theta}) \tag{20b}$$

$$u_q^{+} = U_{+}\sin(\omega t - \hat{\theta}) + U_{-}\sin(-\omega t + \phi^{-1} - \hat{\theta}) \tag{21a}$$

$$u_q^{-} = U_{+}\sin(\omega t + \hat{\theta}) + U_{-}\sin(-\omega t + \phi^{-1} + \hat{\theta}) \tag{21b}$$

we can express (20a) to (21b) in matrices as,

$$\mathbf{u}^{+} = \begin{bmatrix} u_d^{+} \\ u_q^{+} \end{bmatrix} = U_{+}\begin{bmatrix} \cos(\omega t - \hat{\theta}) \\ \sin(\omega t - \hat{\theta}) \end{bmatrix} + U_{-}\begin{bmatrix} \cos(-\omega t + \phi^{-1} - \hat{\theta}) \\ \sin(-\omega t + \phi^{-1} - \hat{\theta}) \end{bmatrix} \tag{22a}$$

$$\mathbf{u}^{-} = \begin{bmatrix} u_d^{-} \\ u_q^{-} \end{bmatrix} = U_{+}\begin{bmatrix} \cos(\omega t + \hat{\theta}) \\ \sin(\omega t + \hat{\theta}) \end{bmatrix} + U_{-}\begin{bmatrix} \cos(-\omega t + \phi^{-1} + \hat{\theta}) \\ \sin(-\omega t + \phi^{-1} + \hat{\theta}) \end{bmatrix} \tag{22b}$$

By the correct tuning of the control loop, the estimated angle $\hat{\theta}$ of the positive sequence voltage vector should be equal to the real angle of this vector, θ. So, $\hat{\theta} = \int \hat{\omega} dt \approx \theta = \int \omega dt$ will result the following voltages from (20a) and (20b),

$$u_d^{+} = U_{+} + U_{-}\cos(-2\omega t + \phi^{-1}) \tag{23a}$$

$$u_d^{-} = U_{+}\cos(2\omega t) + U_{-}\cos(\phi^{-1}) \tag{23b}$$

where $(-\omega t - \phi^{-1} - \hat{\theta}) \approx (-2\omega t - \phi^{-1})$ and $\cos(\omega t - \hat{\theta}) \approx 1$ approximations has been made. Now from (21a) and (21b),

$$u_q^{+} = U_{-}\sin(-2\omega t + \phi^{-1}) \tag{24a}$$

$$u_q^{-} = U_{+}\sin(-2\omega t + \phi^{-1}) + U_{-}\sin(\phi^{-1}) \tag{24b}$$

where $(-\omega t - \phi^{-1} - \hat{\theta}) \approx (-2\omega t - \phi^{-1})$ and $\sin(\omega t - \hat{\theta}) \approx 0$ approximations has been made. Now (22a) and (22b) will be respectively,

$$\mathbf{u}^{+} = \begin{bmatrix} u_d^{+} \\ u_q^{+} \end{bmatrix} = \underbrace{U_{+}\begin{bmatrix} 1 \\ 0 \end{bmatrix}}_{dc\ terms} + \underbrace{U_{-}\begin{bmatrix} \cos(-2\omega t + \phi^{-1}) \\ \sin(-2\omega t + \phi^{-1}) \end{bmatrix}}_{ac\ terms} \tag{25a}$$

$$\mathbf{u}^{-} = \begin{bmatrix} u_d^{-} \\ u_q^{-} \end{bmatrix} = \underbrace{U_{+}\begin{bmatrix} \cos(2\omega t) \\ \sin(2\omega t) \end{bmatrix}}_{ac\ terms} + \underbrace{U_{-}\begin{bmatrix} \cos(\phi^{-1}) \\ \sin(\phi^{-1}) \end{bmatrix}}_{dc\ terms} \tag{25b}$$

In (25a) and (25b), the dc values on the $\mathbf{u}^+$ and the $\mathbf{u}^-$ axes depends on the amplitude of U_+ and U_-, respectively. The term 2ω represents the oscillation as a result of coupling between two axes; because the vectors are rotating in opposite direction. This oscillation is acting as a perturbation for the detection of U_+ and U_-. These oscillations can be attenuated by using traditional filtering techniques. But the grid condition requires high accuracy and excellent dynamic response like dynamic voltage restorers (DVR) under unbalance, conventional SRF-PLL technique is not an appropriate solution for the control of power converters.

5.2 The Decoupling Network

A voltage vector $\mathbf{u}^s$ having two generic components rotating with $n\omega$ and $m\omega$ frequencies respectively, where n and m can be either positive or negative and ω is the fundamental frequency can be expressed as,

$$\mathbf{u}^s = \mathbf{u}^s_n + \mathbf{u}^s_m = U_n \begin{bmatrix} \cos(n\omega t + \phi^n) \\ \sin(n\omega t + \phi^n) \end{bmatrix} + U_m \begin{bmatrix} \cos(m\omega t + \phi^m) \\ \sin(m\omega t + \phi^m) \end{bmatrix} \tag{26}$$

Two rotating reference frames, dq^n reference frame with angular position $n\hat{\theta}$ will be synchronized with $\mathbf{u}^s_n$ and second one is dq^m reference frame with angular position $m\hat{\theta}$ will be synchronized with $\mathbf{u}^s_m$. By the feasible tuning of the control loop, a perfect synchronization of the PLL is possible; where $\hat{\theta} = \int \hat{\omega} dt$ and the reference frames can be written as,

$$\mathbf{u}^n = \begin{bmatrix} u^n_d \\ u^n_q \end{bmatrix} = \begin{bmatrix} \overline{u}^n_d \\ \overline{u}^n_q \end{bmatrix} + \begin{bmatrix} \tilde{u}^n_d \\ \tilde{u}^n_q \end{bmatrix} = \underbrace{U_n \begin{bmatrix} \cos\phi^n \\ \sin\phi^n \end{bmatrix}}_{dc\ terms}$$
$$\underbrace{+ U_m \cos\phi^m \begin{bmatrix} \cos(n-m)\omega t \\ -\sin(n-m)\omega t \end{bmatrix} + U_m \sin\phi^m \begin{bmatrix} \sin(n-m)\omega t \\ \cos(n-m)\omega t \end{bmatrix}}_{ac\ terms} \tag{27}$$

$$\mathbf{u}^m = \begin{bmatrix} u^m_d \\ u^m_q \end{bmatrix} = \begin{bmatrix} \overline{u}^m_d \\ \overline{u}^m_q \end{bmatrix} + \begin{bmatrix} \tilde{u}^m_d \\ \tilde{u}^m_q \end{bmatrix} = \underbrace{U_m \begin{bmatrix} \cos\phi^m \\ \sin\phi^m \end{bmatrix}}_{dc\ terms}$$
$$\underbrace{+ U_n \cos\phi^n \begin{bmatrix} \cos(n-m)\omega t \\ \sin(n-m)\omega t \end{bmatrix} + U_n \sin\phi^n \begin{bmatrix} -\sin(n-m)\omega t \\ \cos(n-m)\omega t \end{bmatrix}}_{ac\ terms} \tag{28}$$

From (27) and (28) it is clearly seen that the amplitude of ac terms in dq^n depends on the dc terms of the signal on the dq^m axes and vice versa. For cancelling out the oscillating term in the dq^n axes, the decoupling cell in Fig. 7 can be used [8]. Also, For cancelling out the oscillating term in the dq^m axes, decoupling cell in Fig. 8 can be used, which is similar to the Fig. 7 but only the position of m and n needs to be interchanged. Now, for estimating the dc values of the positive and negative

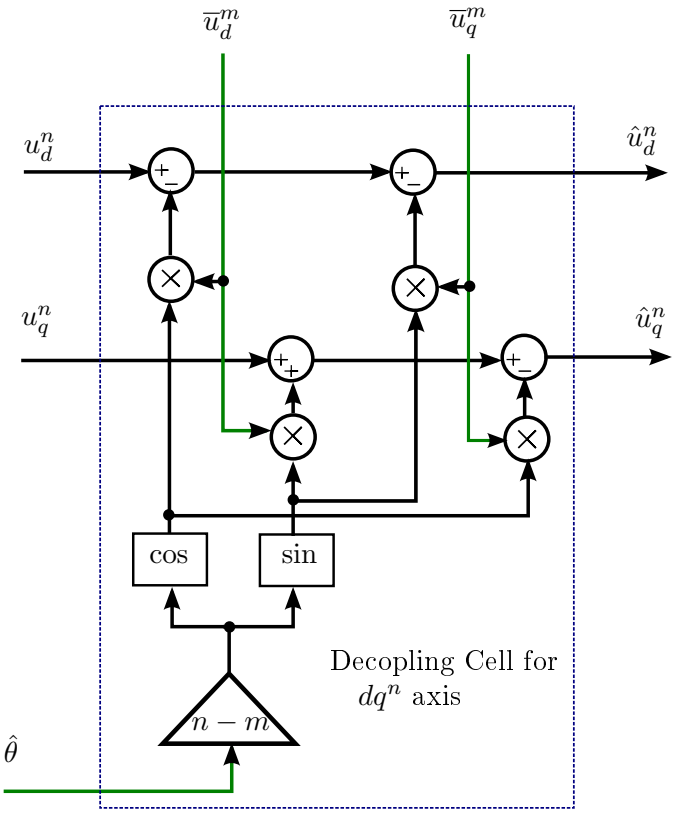

Figure 7: Decoupling cell for cancelling the oscillation on dq^n axes.

reference frames, a cross-feedback decoupling network can be used as shown in Fig. 9. The LPF block is a low pass filter can be represented as [8],

$$LPF(s) = \frac{\omega_f}{s+\omega_f} \tag{29}$$

where, $\omega_f = \frac{\omega}{\sqrt{2}}$ is the cut-off frequency of the LPF and the value of ω_f is selected according to the analysis in [8].

The equations for both decoupling cells can be written as,

$$\overline{u}_d^n = \frac{\omega_f}{s+\omega_f}(u_d^n - \overline{u}_d^m \cos(n-m)\hat{\theta} - \overline{u}_q^m \sin(n-m)\hat{\theta}) \tag{30a}$$

$$\overline{u}_q^n = \frac{\omega_f}{s+\omega_f}(u_q^n + \overline{u}_d^m \sin(n-m)\hat{\theta} - \overline{u}_q^m \cos(n-m)\hat{\theta}) \tag{30b}$$

$$\overline{u}_d^m = \frac{\omega_f}{s+\omega_f}(u_d^m - \overline{u}_d^n \cos(n-m)\hat{\theta} + \overline{u}_q^n \sin(n-m)\hat{\theta}) \tag{30c}$$

$$\overline{u}_q^m = \frac{\omega_f}{s+\omega_f}(u_q^m - \overline{u}_d^n \sin(n-m)\hat{\theta} - \overline{u}_q^n \cos(n-m)\hat{\theta}) \tag{30d}$$

Now considering an unbalance voltage during a grid fault, consisting of positive and negative sequence components at fundamental frequency, where $n=1$ and $m=-1$, (26) can be represented as,

$$\mathbf{u}^s = \mathbf{u}^s_{+1} + \mathbf{u}^s_{-1} = U_{+1}\begin{bmatrix} \cos(\omega t + \phi^{+1}) \\ \sin(\omega t + \phi^{+1}) \end{bmatrix} + U_{-1}\begin{bmatrix} \cos(-\omega t + \phi^{-1}) \\ \sin(-\omega t + \phi^{-1}) \end{bmatrix} \tag{31}$$

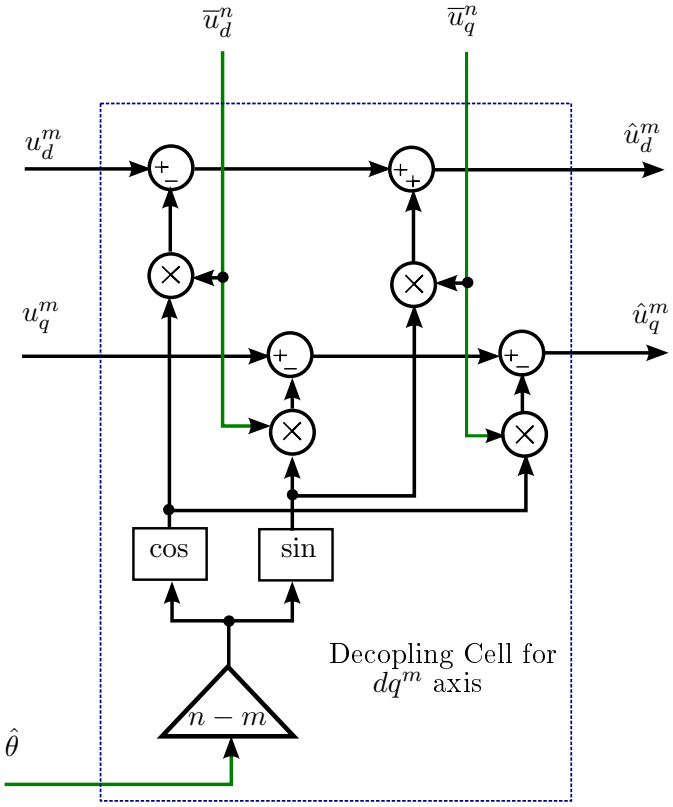

Figure 8: Decoupling cell for cancelling the oscillation on dq^m axes

Then (27) will be,

$$\begin{aligned}\mathbf{u}^{+1} &= U_{+1}\begin{bmatrix}\cos\phi^{+1}\\ \sin\phi^{+1}\end{bmatrix} + U_{-1}\cos\phi^{-1}\begin{bmatrix}\cos 2\omega t\\ -\sin 2\omega t\end{bmatrix} + U_{-1}\sin\phi^{-1}\begin{bmatrix}\sin 2\omega t\\ \cos 2\omega t\end{bmatrix}\\ &= U_{+1}\begin{bmatrix}\cos\phi^{+1}\\ \sin\phi^{+1}\end{bmatrix} + U_{-1}\begin{bmatrix}\cos 2\omega t & \sin 2\omega t\\ -\sin 2\omega t & \cos 2\omega t\end{bmatrix}\begin{bmatrix}\cos\phi^{-1}\\ \sin\phi^{-1}\end{bmatrix} \end{aligned} \quad (32)$$

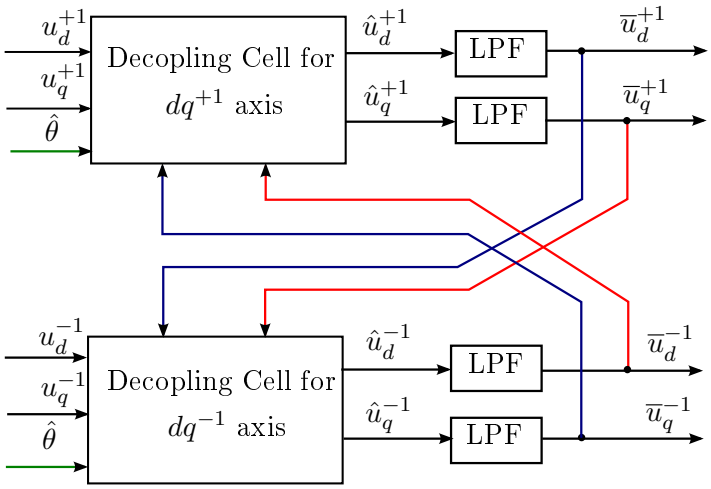

Figure 9: Decoupling network of dq^n and dq^m reference frames.

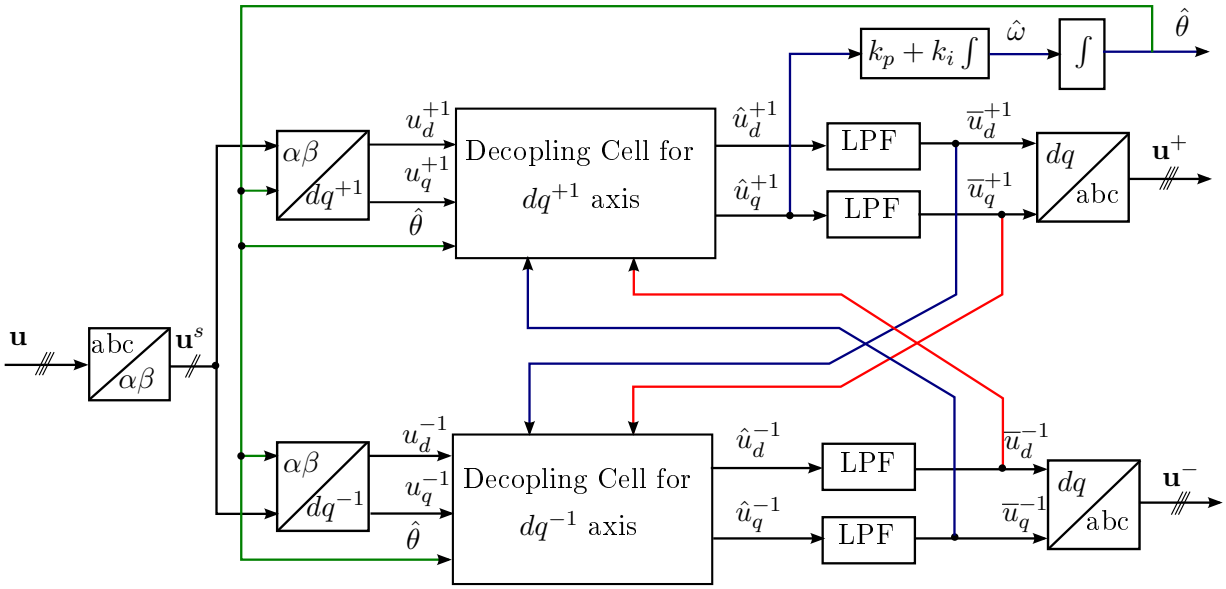

Figure 10: Block diagram of the decoupled double synchronous reference frame PLL (DSRF-PLL).

and (28) will be,

$$\begin{aligned}\mathbf{u}^{-1} &= U_{-1}\begin{bmatrix}\cos\phi^{-1}\\ sin\phi^{-1}\end{bmatrix} + U_{+1}\cos\phi^{+1}\begin{bmatrix}\cos 2\omega t\\ \sin 2\omega t\end{bmatrix} + U_{+1}\sin\phi^{+1}\begin{bmatrix}-\sin 2\omega t\\ \cos 2\omega t\end{bmatrix}\\ &= U_{-1}\begin{bmatrix}\cos\phi^{-1}\\ \sin\phi^{-1}\end{bmatrix} + U_{+1}\begin{bmatrix}\cos 2\omega t & -\sin 2\omega t\\ \sin 2\omega t & \cos 2\omega t\end{bmatrix}\begin{bmatrix}\cos\phi^{+1}\\ \sin\phi^{+1}\end{bmatrix}\end{aligned} \tag{33}$$

(30a), (30b), (30c) and (30d) can be written as respectively where $\hat{\theta} = \int \hat{\omega} dt$,

$$\overline{u}_d^{+1} = \frac{\omega_f}{s+\omega_f}(u_d^{+1} - \overline{u}_d^{-1}\cos 2\omega t - \overline{u}_q^{-1}\sin 2\omega t) \tag{34a}$$

$$\overline{u}_q^{+1} = \frac{\omega_f}{s+\omega_f}(u_q^{+1} + \overline{u}_d^{-1} sin2\omega t - \overline{u}_q^{-1} cos2\omega t) \tag{34b}$$

$$\overline{u}_d^{-1} = \frac{\omega_f}{s+\omega_f}(u_d^{-1} - \overline{u}_d^{+1} cos2\omega t + \overline{u}_q^{+1} sin2\omega t) \tag{34c}$$

$$\overline{u}_q^{-1} = \frac{\omega_f}{s+\omega_f}(u_q^{-1} - \overline{u}_d^{+1} sin2\omega t - \overline{u}_q^{+1} cos2\omega t) \tag{34d}$$

The decoupling network in Fig. 10 completely cancels out the double frequency oscillations at 2ω on the dq^{+1} and dq^{-1} reference frame signals; the control loop bandwidth is no need to be reduced and the real amplitude of the unbalanced input voltage sequence components can be exactly detected [1]. With these decoupling networks, the signal with frequency 2ω does not arrive in the PI controller input, and hence the system bandwidth can be increased for achieving a better dynamic behavior.

6 Second-order Generalized Integrator Frequency Locked Loop (SOGI-FLL)

PLL technique based on SRF has become a conventional way for grid synchronization. The response of the SRF-PLL is not really acceptable during unbalanced fault condition, because of the appearance of negative sequence in the voltage. As a result, the SRF-PLL method has been modified with different synchronization technique. Nevertheless, the dynamic response of the PLL method can be sensitive during a fault, as the phase angle jumps in the voltage at the PCC and PLL is synchronized with phase angle. For avoiding this phenomenon, a technique based on the frequency locked loop (FLL) is a substantial solution [9]. The FLL estimates the frequency of an input signal, which is not affected by sudden phase angle changes and might be advantageous than PLL based algorithms in that case.

The FLL technique is based on the second-order generalized integrator (SOGI), which works as a processing block of an adaptive filter. The SOGI is self tuned by the means of a FLL and together as a grid synchronization system, is called SOGI-FLL [9]. Control algorithm of a SOGI-FLL mainly combines with these following concepts.

1. Adaptive filter (AF)
2. Generalized integrator (GI)
3. Second-order generalized integrator (SOGI)
4. Frequency locked loop (FLL)

6.1 Generalized Integrator (GI)

The GI is the base of proportional-resonant (PR) controllers. The basic function of a PR controller is to introduce an infinite gain at a selected resonant frequency for eliminating the steady-state error at that frequency, which is conceptually similar to an integrator whose infinite dc gain forces the dc steady-state error to zero. So the resonant part of the PR controller can be called as a generalized integrator (GI) [15].

Time domain convolution product of a sinusoidal function by itself gives rise to a sinusoidal term multiplied by the time variable. Output contains not only the integration of the input, but also an additional negligible component. Fig. 11 shows a generalized integrator for a single sinusoidal signal in part (a) and the corresponding stationary-frame generalized integrator in part (b), which works without regard to the sequence between the α-axis signal and the β-axis signal [14].

Generalized integrator (GI) has the ability to generate a set of in-quadrature signal orthogonal to each other, known as, quadrature signals generator (QSG). These can be used to estimate the rms value of the grid voltage and current for calculate

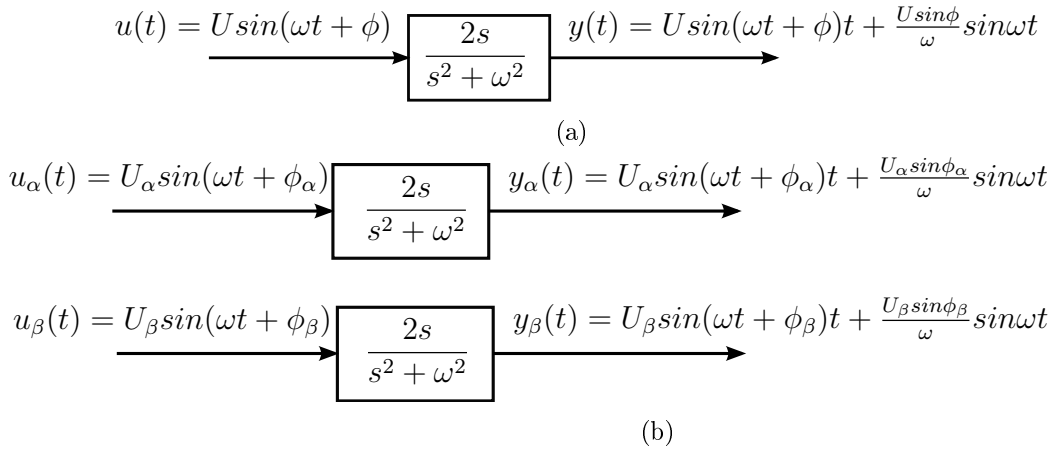

Figure 11: (a) The generalized integrator for a single sinusoidal signal (b) The corresponding stationary-frame generalized integrator. The stationary-frame generalized integrator works without regard to the sequence between the α-axis signal and the β-axis signal.

the active and reactive power references and also for calculate the positive- and negative-sequence components in three phase systems.

6.2 AF based on SOGI

A single frequency adaptive noise canceller based on an adaptive filter (AF) in the continuous time domain is shown in Fig. 13. The AF portion of this Fig. 13 is similar to Fig. 12, which is presented in [16]. The idea of this construction in Fig. 12 is based on product demodulation method [16], which is related to traditional Park's transformation for three phase systems and its fundamentals are well known in spectrum analysis theory. Here the signal is multiplied by reference sine and cosine waveforms which shift any harmonic content at that frequency to dc and the double-frequency. The integrators in Fig. 12 does double role of providing integral action and filtering the double-frequency components for the demodulated signal.

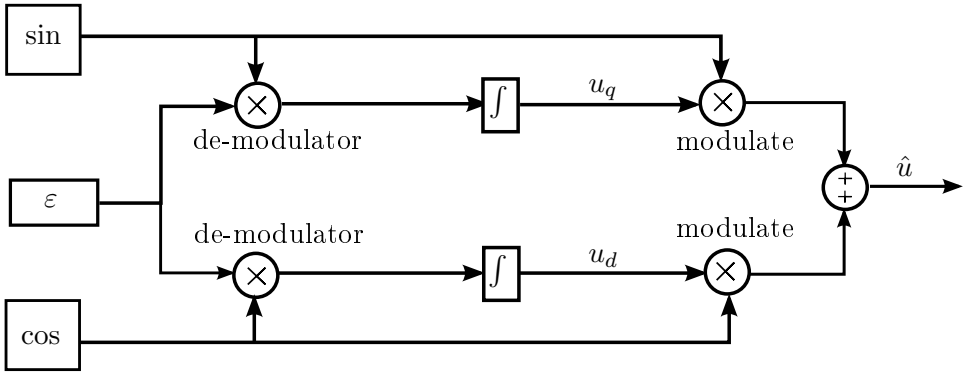

Figure 12: Demodulating single-phase integral block.

In Fig. 13 it is evident that the auxiliary signal $\hat{\omega}$ is responsible for setting the frequency of the sinusoidal interference to be cancelled from the primary input signal u. In this system, $\hat{\omega}$ is taken as the reference signal and frequency to be filtered.

u_d and u_q signals of Fig. 13 can be written as, which is similar as the mathematical expression (Euler's relation) for Fig. 12.

$$u_d = k\varepsilon_u \cos\hat{\omega}t = \frac{1}{2}k\varepsilon_u \left[e^{j\hat{\omega}t} + e^{-j\hat{\omega}t}\right] \tag{35}$$

$$u_d = k\varepsilon_u \sin\hat{\omega}t = \frac{1}{j2}k\varepsilon_u \left[e^{j\hat{\omega}t} - e^{-j\hat{\omega}t}\right] \tag{36}$$

where ε_u is synchronization error signal. Let $h = k\varepsilon_u$. A_d and A_q in Fig. 13 corresponds to the output of the integrators for $\hat{u}_d$ and $\hat{u}_q$ respectively, can be expressed in Laplace domain as [1],

$$A_d(s) = \frac{1}{s}u_d(s) = \frac{1}{2}\left[h(s + j\hat{\omega}t) + h(s - j\hat{\omega}t)\right] \tag{37}$$

$$A_q(s) = \frac{1}{s}u_q(s) = \frac{1}{j2}\left[h(s + j\hat{\omega}t) + h(s - j\hat{\omega}t)\right] \tag{38}$$

The Laplace transformation of $\hat{u}_d$ and $\hat{u}_q$ can be written as,

$$\begin{aligned}\hat{u}_d(s) &= \frac{1}{2}\left[A_d(s + j\hat{\omega}t) + A_d(s - j\hat{\omega}t)\right] \\ &= \frac{1}{4(s + j\hat{\omega})}\left[h(s) + h(s + 2j\hat{\omega})\right] + \frac{1}{4(s - j\hat{\omega})}\left[h(s) + h(s - 2j\hat{\omega})\right]\end{aligned} \tag{39}$$

$$\begin{aligned}\hat{u}_q(s) &= \frac{1}{2j}\left[A_q(s + j\hat{\omega}t) - A_q(s - j\hat{\omega}t)\right] \\ &= \frac{1}{4(s + j\hat{\omega})}\left[h(s) - h(s + 2j\hat{\omega})\right] + \frac{1}{4(s - j\hat{\omega})}\left[h(s) - h(s - 2j\hat{\omega})\right]\end{aligned} \tag{40}$$

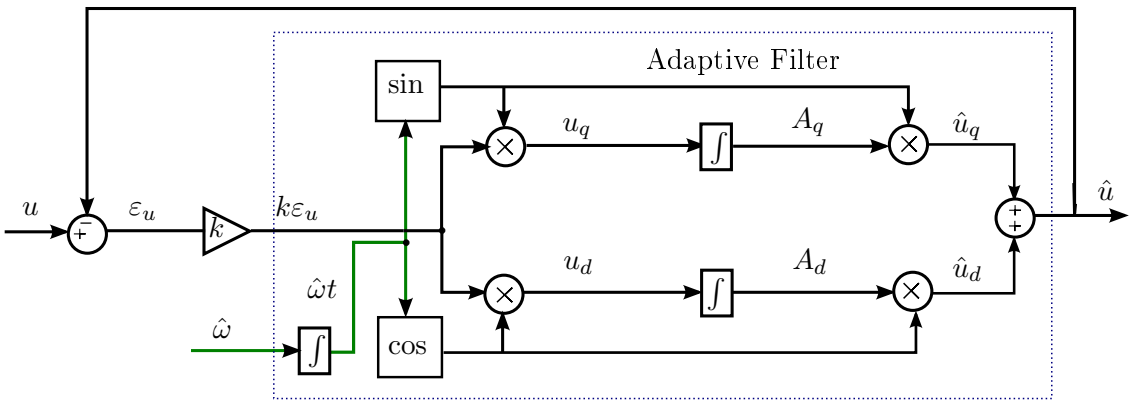

Figure 13: Single-frequency adaptive noise canceller.

Now if we add (39) and (40), we will get the output $\hat{u}$ as,

$$\hat{u}(s) = \hat{u}_d(s) + \hat{u}_q(s) = \frac{s}{s^2 + \hat{\omega}^2} h(s) \tag{41}$$

If $\hat{u}$ and $k\varepsilon_u$ are the output and input signal respectively, then the transfer function for AF structure in Fig. 13 can be written as,

$$AF(s) = \frac{\hat{u}}{k\varepsilon_u}(s) = \frac{s}{s^2 + \hat{\omega}^2} \tag{42}$$

Now we can see that the transfer function of (42) matches the transfer function of Fig.11 which is a GI for sinusoidal signals. Another feature of the system of Fig. 13 is that this system can be used as a quadrature signal generator (QSG) by just adding a scaled integrator at the output of it which will generate another signal with 90^0 phase shift.

Fig. 14 shows an AF based on a GI. The filtering structures in Fig. 13 and Fig. 14 are equivalent and both will give the same dynamic performance when working as an adaptive noise canceller.

The transfer function of two in-quadrature output signals of the AF in Fig. 14 can be written as,

$$D(s) = \frac{\hat{u}}{u}(s) = \frac{ks}{s^2 + ks + \hat{\omega}^2} \tag{43}$$

$$Q(s) = \frac{q\hat{u}}{u}(s) = \frac{k\hat{\omega}^2}{s^2 + ks + \hat{\omega}^2} \tag{44}$$

where $\hat{\omega}$ is the tuning frequency; k is the damping factor of the filter; $\hat{u}$ and $q\hat{u}$ are the in-phase and in-quadrature signals of the input u with a phase shift of 90^o. The component $\hat{u}$ has the same phase and magnitude as the fundamental of the input signal u.

As we can see from the transfer functions of (43) and (44), the bandwidth of the band-pass filter given by (43) and the steady-state gain of low-pass filter given by

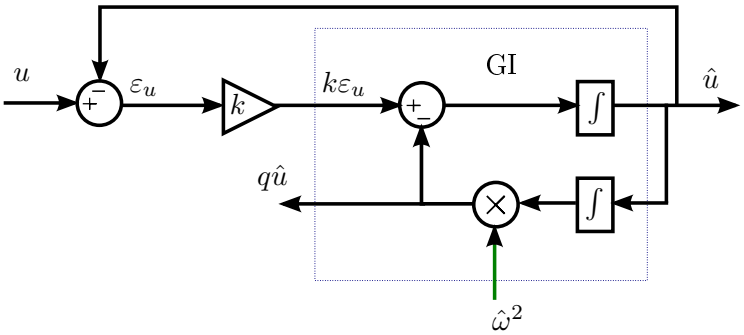

Figure 14: Structure of AF based on GI.

(44) are not only a function of the gain k, but also depend on the center frequency of the filter $\hat{\omega}$ which is the resonance frequency of the GI [9].

A solution for this kind of problem was addressed by Mojiri et al. in [17]. Using the same method, here we can multiply the input signal u by $\hat{\omega}^2$ and the feedback signal $\hat{u}$ by $\hat{\omega}$. This is shown in Fig. 15 and the transfer functions from the figure are,

$$D(s) = \frac{\hat{u}}{u}(s) = \frac{k\hat{\omega}^2 s}{s^2 + ks + \hat{\omega}^2} \tag{45}$$

$$Q(s) = \frac{q\hat{u}}{u}(s) = \frac{k\hat{\omega}^4}{s^2 + ks + \hat{\omega}^2} \tag{46}$$

From (45) and (46) we can see that they are independent of the center frequency $\hat{\omega}$ which is set by the gain k. But in the case of $\hat{\omega} = \omega$, the amplitude of both $\hat{u}$ and $q\hat{u}$ will not match with the amplitude of input u. For solving this problem an alternative solution was presented by Mojiri et al. in [18], which is shown in Fig. 16. We can write the transfer functions as below,

$$D(s) = \frac{\hat{u}}{u}(s) = \frac{k\hat{\omega} s}{s^2 + ks + \hat{\omega}^2} \tag{47}$$

$$Q(s) = \frac{q\hat{u}}{u}(s) = \frac{k\hat{\omega}^2}{s^2 + ks + \hat{\omega}^2} \tag{48}$$

From (47) and (48) we can see that the bandwidth of the AF depends only on the gain k. Also the amplitude of two in-quadrature signals $\hat{u}$ and $q\hat{u}$ will be the same as the amplitude of the signal u, when $\hat{\omega} = \omega$.

Fig. 16 is looking quite complicated by structure and the detected frequency $\hat{\omega}$ need to be squared. So after some modification of the AF structure, a new structure is shown in Fig. 17 [20]. It also exhibits the same dynamic response and transfer functions. This new sinusoidal integrator is called SOGI and have the ability to

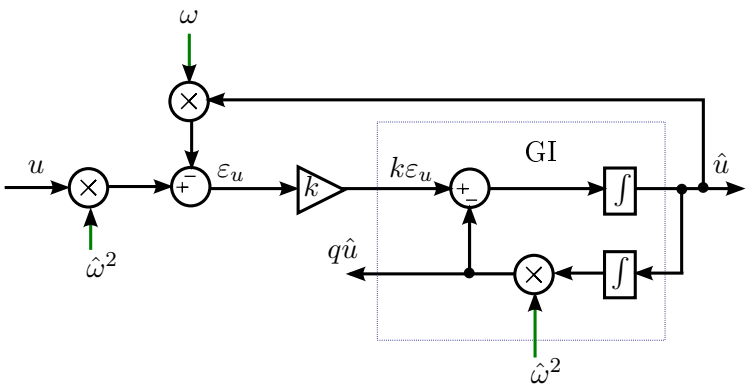

Figure 15: Structure of AF based on GI with a bandwidth independent of the frequency $\hat{\omega}$.

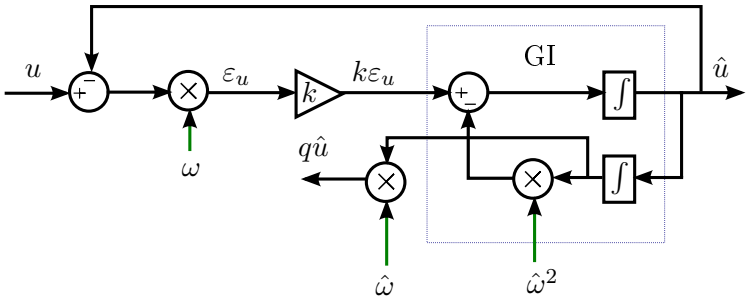

Figure 16: Structure of AF based on GI with a bandwidth independent of the frequency $\hat{\omega}$ and normalized output amplitude.

work as a QSG [19]. The transfer function for SOGI is given below, which is similar as (42) and the transfer functions shown in Fig. 11.

$$SOGI(s) = \frac{\hat{u}}{k\varepsilon_u}(s) = \frac{\hat{\omega}s}{s^2 + \hat{\omega}^2} \tag{49}$$

6.3 SOGI Frequency-Locked Loop

The natural resonant characteristic of the SOGI makes itself work as a VCO. This phenomenon gives a idea of designing a simple control loop to auto-adapt the center frequency of the SOGI resonator to the input frequency. This is the main idea of introducing the frequency-locked loop (FLL) [1]. The center frequency $\hat{\omega}$ of the structures in Fig. 17 should be adapted to the frequency of the input signal ω for generating a balanced set of in-quadrature outputs with the same amplitudes. In order to make the SOGI structure auto-tunable, analysis of the error signal ε_u is needed to regulate the center frequency $\hat{\omega}$. The transfer function from the input signal u to the error signal ε_u can be written as,

$$E(s) = \frac{\varepsilon_u}{u}(s) = \frac{s^2 + \hat{\omega}^2}{s^2 + k\hat{\omega}s + \hat{\omega}^2} \tag{50}$$

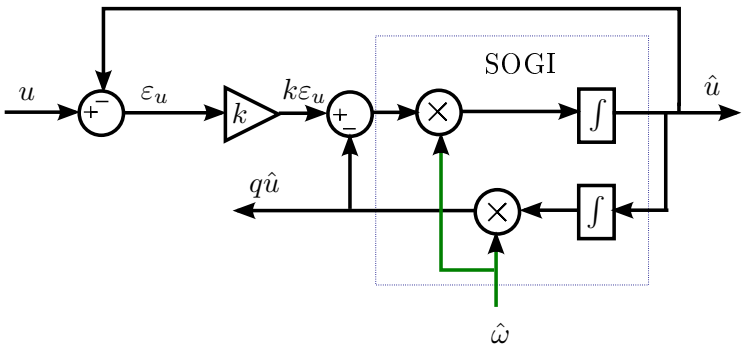

Figure 17: Structure of the SOGI.

The transfer function in (50) of Fig. 17 respond to a second order notch filter, with zero gain at the center frequency. The Bode diagrams of (50) for $E(s)$ (which is similar to a bode diagram of a second order notch filter) and (48) for $Q(s)$ are shown in Fig. 18. Here the signal ε_u and $q\hat{u}$ are in phase when the input frequency ω is lower than the SOGI resonance frequency $\hat{\omega}$, is that $\omega < \hat{\omega}$ and they are in counter-phase when $\omega > \hat{\omega}$. Now, if we define a frequency error variable ε_f, which is the product of ε_u and $q\hat{u}$, then, the average value of ε_f is positive for $\omega < \hat{\omega}$, zero for $\omega = \hat{\omega}$ and negative for $\omega > \hat{\omega}$, which is also shown in Fig. 18.

According to the behavior of ε_f with ω and $\hat{\omega}$, an integral controller with a negative gain $-\gamma$ can be used to cancel the dc component of ε_f by shifting the SOGI resonance frequency $\hat{\omega}$ which is shown in Fig. 19. After that if we add this integral value (which can be either positive or negative, depending on the changes of frequency) with the nominal value of the grid frequency as a feed-forward variable ω_{ff}, then we will get $\hat{\omega}$ and it will match the input frequency ω by this synchronization process.

This unique combination of the SOGI and the FLL together, which is shown in Fig. 19, gives a single-phase grid synchronization system known as SOGI-FLL [9]. Here in the SOGI-FLL, the input frequency is directly detected by the FLL, while the estimation of the phase angle and the amplitude of the input 'virtual vector' $\hat{\mathbf{u}}$ can be indirectly calculated as,

$$|\hat{\mathbf{u}}| = \sqrt{(\hat{u})^2 + (q\hat{u})^2} \tag{51a}$$

$$\angle\hat{\mathbf{u}} = \arctan\frac{q\hat{u}}{\hat{u}} \tag{51b}$$

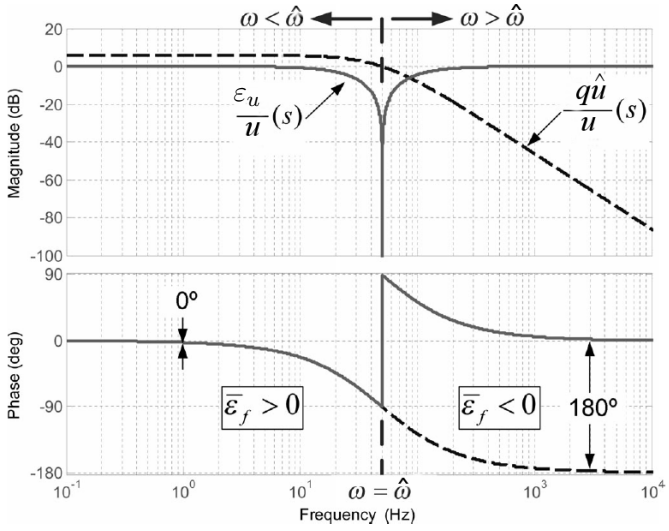

Figure 18: Bode diagram of the FLL input variables. [9].

6.4 Calculation of the Parameters for Tuning the SOGI-FLL

The performance and dynamical response of the SOGI-FLL depends mainly on the accurate selection of the control parameters k and γ, which will satisfy the design specifications. In this section, the equations of the SOGI-FLL will be analysed in order to find the appropriate values for k and γ for achieving the desired performance in the detection of the amplitude and frequency of the input signal.

From Fig. 19, we can identify the state description matrices simply by inspection; this is possible because when the output of an integrator is a state variable, the input of that integrator is the derivative of that variable [21]. So, from Fig. 19, the equation for the first state variable is,

$$\dot{x_1} = -k\hat{\omega}x_1 - \hat{\omega}^2 x_1 + k\hat{\omega}u \tag{52}$$

Continuing in this way, we get

$$\dot{x_2} = x_1 \tag{53a}$$
$$\hat{u} = x_1 \tag{53b}$$
$$q\hat{u} = \hat{\omega}x_2 \tag{53c}$$

(52), (53a), (53b) and (53c) can be rewritten in the matrix form as state-space

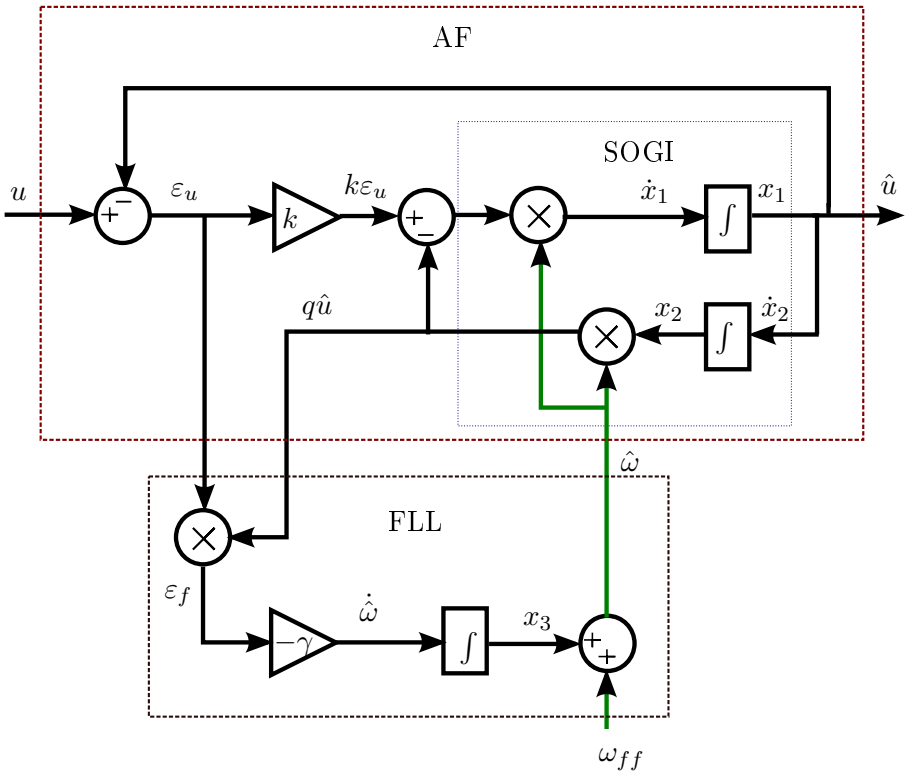

Figure 19: Single-phase grid-synchronization system based on SOGI-FLL.

equations,

$$\dot{\mathbf{x}} = \begin{bmatrix} \dot{x_1} \\ \dot{x_2} \end{bmatrix} = \mathbf{A}\mathbf{x} + \mathbf{B}u = \begin{bmatrix} -k\hat{\omega} & -\hat{\omega}^2 \\ 1 & 0 \end{bmatrix} \begin{bmatrix} x_1 \\ x_2 \end{bmatrix} + \begin{bmatrix} k\hat{\omega} \\ 0 \end{bmatrix} u \tag{54a}$$

$$\mathbf{y} = \begin{bmatrix} \hat{u} \\ q\hat{u} \end{bmatrix} = \mathbf{C}\mathbf{x} = \begin{bmatrix} 1 & 0 \\ 0 & \hat{\omega} \end{bmatrix} \begin{bmatrix} x_1 \\ x_2 \end{bmatrix} \tag{54b}$$

$$\dot{\hat{\omega}} = -\gamma x_2 \hat{\omega}(u - x_1) \tag{54c}$$

where $\mathbf{x}$ and $\mathbf{y}$ are the SOGI state and output vectors respectively and the state equation describing the behaviour of the FLL is shown in (54c). For symbolic notation, matrices are shown by the use of bold type. Now, if we consider normal operating conditions, which gives $\dot{\hat{\omega}} = 0$ and $\omega = \hat{\omega}$ and $x_1 = u$, then (54a) can be rewritten as,

$$\dot{\overline{\mathbf{x}}} = \begin{bmatrix} \dot{\overline{x}}_1 \\ \dot{\overline{x}}_2 \end{bmatrix} = \begin{bmatrix} 0 & -\hat{\omega}^2 \\ 1 & 0 \end{bmatrix} \begin{bmatrix} x_1 \\ x_2 \end{bmatrix} \tag{55}$$

where the steady-state variables are identified by a bar over. The eigenvalues of the Jacobian, which can be obtained from (55), are complex conjugate with a null real part, ensure the resonant behaviour of the system, as the steady-state response remains in a periodic orbit at the $\hat{\omega}$ frequency. So, if $u = U\sin(\omega t + \phi)$ is an input signal, the steady state output vector will be,

$$\overline{\mathbf{y}} = \begin{bmatrix} \hat{u} \\ q\hat{u} \end{bmatrix} = U \begin{bmatrix} \sin(\omega t + \phi) \\ -\cos(\omega t + \phi) \end{bmatrix} \tag{56}$$

6.4.1 Tuning of SOGI

The value of gain k can be selected from (57), which is shown from an analysis in [9]:

$$t_{\text{SOGI}} = \frac{10}{k\hat{\omega}} \tag{57}$$

where t_{SOGI} is the settling time for SOGI. From (57), we can see that the higher the value k, the faster the response of the SOGI. The value of k also affects the bandwidth of the SOGI; the higher value k would make the performance of SOGI fast but reducing its immunity in the case of harmonics on the input, and a lower value of k can cause a very long undamped transient response of the SOGI. So, considering all the circumstances and after a signal analysis in [9], the value is selected as $k = \sqrt{2}$. It is worth mentioning that the gain $k = \sqrt{2}$ say indirectly a damping factor $\xi = \frac{1}{\sqrt{2}}$, which roughly results in an ideal relationship between the settling time and overshooting in the dynamic response.

6.4.2 Tuning of FLL

The input signal of SOGI is assumed sinusoidal at the frequency ω and even in the case of $\omega \neq \hat{\omega}$, the state variables of SOGI-QSG have the following relationship [11],

$$\dot{\overline{x}}_1 = -\omega^2 \dot{\overline{x}}_2 \tag{58}$$

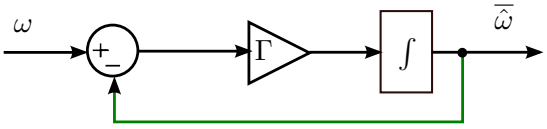

Figure 20: Simplified frequency adaption system of FLL.

Now the steady-state synchronization error signal can be written as from (54a),

$$\overline{\varepsilon}_u = u - \dot{\overline{x}}_1 = \frac{1}{k\hat{\omega}}(\dot{\overline{x}}_1 + \hat{\omega}^2\overline{x}_2) \tag{59}$$

From (58) and (59), the steady-state frequency error signal $\overline{\varepsilon}_f$ can be written as,

$$\overline{\varepsilon}_f = \hat{\omega}\overline{x}_2\overline{\varepsilon}_u = \frac{\overline{x}_2^2}{k}(\hat{\omega}^2 - \omega^2) \tag{60}$$

Expression (60) shows that the signal $\overline{\varepsilon}_f$ collects information about error in frequency estimation, and hence, it is suitable to act as the control signal of the FLL. Nevertheless, expression (60) is highly nonlinear, which means linear control analysis techniques cannot directly be applied to set the value of the FLL gain, γ. As demonstrated in [25], the averaged dynamics of the FLL with $\omega \approx \hat{\omega}$ can be written as,

$$\dot{\overline{\hat{\omega}}} = -\frac{\gamma U^2}{k\hat{\omega}}(\dot{\hat{\omega}} - \omega) \tag{61}$$

Equation (61) shows the relationship between the dynamic response of the FLL, the SOGI-QSG gain and the parameters of input signal. From (61), the value of γ can be normalized as shown in (62) by using feedback variables [25]. This gives a first-order linearized frequency adaptive system, which does not dependent on neither the grid variables nor the SOGI-QSG gain and shown in Fig. 20.

$$\gamma = -\frac{k\hat{\omega}}{U^2}\Gamma \tag{62}$$

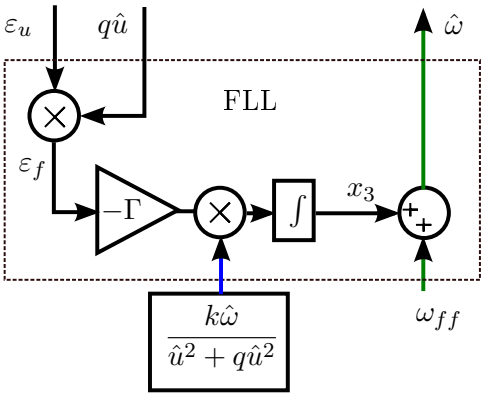

Figure 21: SOGI-FLL with FLL gain normalization

The transfer function of the first-order frequency adaptation loop of Fig. 20 can be written as,

$$\frac{\overline{\hat{\omega}}}{\omega} = -\frac{\Gamma}{s+\Gamma} \tag{63}$$

So, the settling time is purely depend on Γ and can be calculated by [21] as,

$$t_{\mathrm{FLL}} = \frac{5}{\Gamma} \tag{64}$$

feedback-based linearized FLL is shown in Fig. 21. In this system, the FLL gain is adjusted in runtime by feeding back the estimated grid operating conditions, which confirms constant settle time in grid frequency estimation independently of input signal characteristics.

A simulation analysis in [9] shows that for $\Gamma = 50$ give the settling time $t_{\mathrm{FLL}} =$ 100 ms with the error is within 5% just after 20 ms, which is acceptable and will be used for the simulation in this thesis.

7 Double Second-order Generalized Integrator Frequency Locked Loop (DSOGI-FLL)

In previous section, SOGI-FLL single-phase algorithm has been modeled and tuned accordingly. In this section, SOGI-FLL will be modelled for three-phase grid synchronization applications and called as DSOGI-FLL. This synchronization algorithm allows estimating of the instantaneous symmetrical components of the grid voltage in the $\alpha\beta$ domain and also the frequency value.

7.1 Positive- and Negative-sequence Calculation on the $\alpha\beta$ Reference Frame

The instantaneous positive- and negative-sequence voltage components on the $\alpha\beta$ reference frame can be calculated by using Lyon's transformations, which is presented in [26]:

$$\begin{aligned} \mathbf{u}^s_+ &= [T_{\alpha\beta}]\,\mathbf{u}_+ \\ &= [T_{\alpha\beta}]\,[T_+]\,\mathbf{u} \\ &= [T_{\alpha\beta}]\,[T_+]\,[T_{\alpha\beta}]^{\mathrm{T}}\,\mathbf{u}^s \\ &= \frac{1}{2}\begin{bmatrix} 1 & -q \\ q & 1 \end{bmatrix}\mathbf{u}^s \end{aligned} \tag{65}$$

$$\begin{aligned} \mathbf{u}^s_- &= [T_{\alpha\beta}]\,\mathbf{u}_- \\ &= [T_{\alpha\beta}]\,[T_-]\,\mathbf{u} \\ &= [T_{\alpha\beta}]\,[T_-]\,[T_{\alpha\beta}]^{\mathrm{T}}\,\mathbf{u}^s \\ &= \frac{1}{2}\begin{bmatrix} 1 & q \\ -q & 1 \end{bmatrix}\mathbf{u}^s \end{aligned} \tag{66}$$

where $[T_+]$ and $[T_-]$ are defined as:

$$[T_+] = \begin{bmatrix} 1 & a & a^2 \\ a^2 & 1 & a \\ a & a^2 & 1 \end{bmatrix};\ [T_-] = \begin{bmatrix} 1 & a^2 & a \\ a & 1 & a^2 \\ a^2 & a & 1 \end{bmatrix}$$

here $a = e^{-j(2\pi/3)}$; and $q = e^{-j(\pi/2)}$ is a 90° lagging phase-shifting operator applied on the time domain to obtain an in-quadrature version of the input waveforms.

7.2 Structure of DSOGI-FLL

The structure of DSOGI-FLL is shown in Fig. 22, where symbols with 'hat' express the estimated value from the system. This unique three-phase grid synchronization system in $\alpha\beta$ domain is modelled with the help of Lyon's transformation, which is shown in (65) and (65). Here in Fig. 22, two SOGIs are needed to compute the symmetrical components in a three-phase application, one for α and another

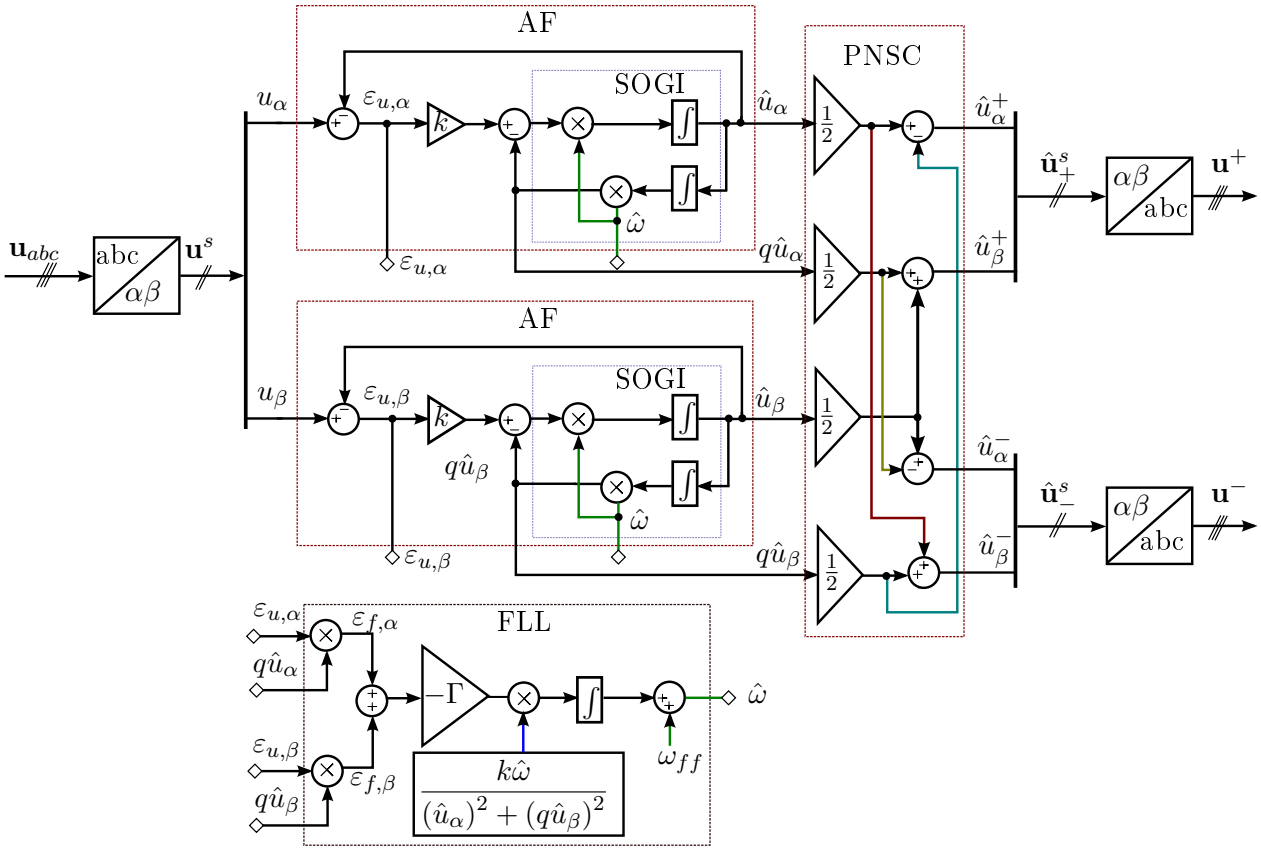

Figure 22: Structure of DSOGI-FLL.

for β. Here two SOGIs are in parallel to give the signal to a positive/negative sequence calculation (PNSC) block to perform the transformation in (65) and (65) [9].

In previous section, SOGI has an independent FLL for frequency estimation. Here for DSOGI implementation, we have two SOGIs and we can use only one FLL for frequency estimation as the frequency of both u_α and u_β signals are always the same. The FLL gain normalization of DSOGI-FLL is done accordingly as for the SOGI-FLL. Here we can see from Fig. 22 that the gain is normalized by squaring the amplitude of both positive-sequence component as u_α^{+2} and u_β^{+2}, which gives a first-order linearized system and have the same response as in (64).

8 Performance of DDSRF-PLL and DSOGI-FLL in Different Grid fault Condition

In previous sections, grid synchronization method based on DDSRF-PLL and DSOGI-PLL has been developed. In this section, the performance of DDSRF-PLL and DSOGI-FLL will be compared in different grid fault conditions. For the comparison, both DDSRF-PLL and DSOGI-FLL are simulated with same characterized input voltage. DDSRF-PLL and DSOGI-FLL synchronization algorithms are modelled by using Matlab Simulink.

8.1 Performance Under Unbalanced Voltage Condition

For unbalanced condition, the input voltage is characterized as $U_+ = 100$ V, $U_- = 30$ V, $\phi^{-1} = 0$ and $\omega = 2\pi 50$ rad/s and appears after 0.5 s, being the prefault grid voltage equal to $U_{\text{pf}} = 100$ V. The values for the PI controller parameters are $k_p = 2.22$ and $k_i = 246.7$, are selected according to [9]; which results $\xi_{\text{PLL}} \approx 1/\sqrt{2}$ and the control loop bandwidth is reduced to $\omega_{\text{PLL}} \approx 2\pi 25$ rad/s. Fig. 23(a) shows the performance of DDSRF-PLL and Fig. 23(b) shows the performance of and DSOGI-FLL. Here in Fig. 23, the estimated positive- and negative-sequence voltage, phase angle and frequency are shown. Both DDSRF-PLL and DSOGI-FLL can perfectly track the unbalanced grid components within 20 ms or in one utility period. The performance of both DDSRF-PLL and DSOGI-FLL are acceptable in this case.

8.2 Performance Under Harmonic-distorted Condition

For evaluating the performance of DDSRF-PLL and DSOGI-FLL under severe utility harmonic-distorted condition, an unbalanced fifth harmonic component characterized as $U_{+5} = 10$ V, $U_{-5} = 10$ V, is added to the utility voltage with the previous characterization as in section 8.1. The control parameters are selected as $k_p = 2.22$ and $k_i = 246.7$. Fig. 24(a) shows the performance of DDSRF-PLL and Fig. 24(b) shows the performance of and DSOGI-FLL. Here we can see that the estimation of the phase angle of the positive-sequence voltage is quite accurate for DDSRF-PLL regardless of the distorted utility voltages. This is because the oscillation in phase angle is attenuated as a consequence of the low-pass characteristic of (16) and the parameters are set as $\omega_{\text{PLL}} \approx 2\pi 25$ rad/s and $\xi_{\text{PLL}} \approx 1/\sqrt{2}$.

The negative-sequence estimation of the voltage for DDSRF-PLL and DSOGI-FLL are disturbed due to the voltage harmonic pollution. The frequency estimation of the DDSRF-PLL is also disturbed due to the voltage harmonic pollution. Meanwhile, the frequency estimation of the DSOGI-FLL does not have much oscillation, because of the adaptive filtering characteristics of DSOGI-FLL. This shows that DDSRF-PLL cannot perform accurately under harmonic-distorted grid voltage and

DSOGI-FLL shows better performance in the case of frequency estimation.

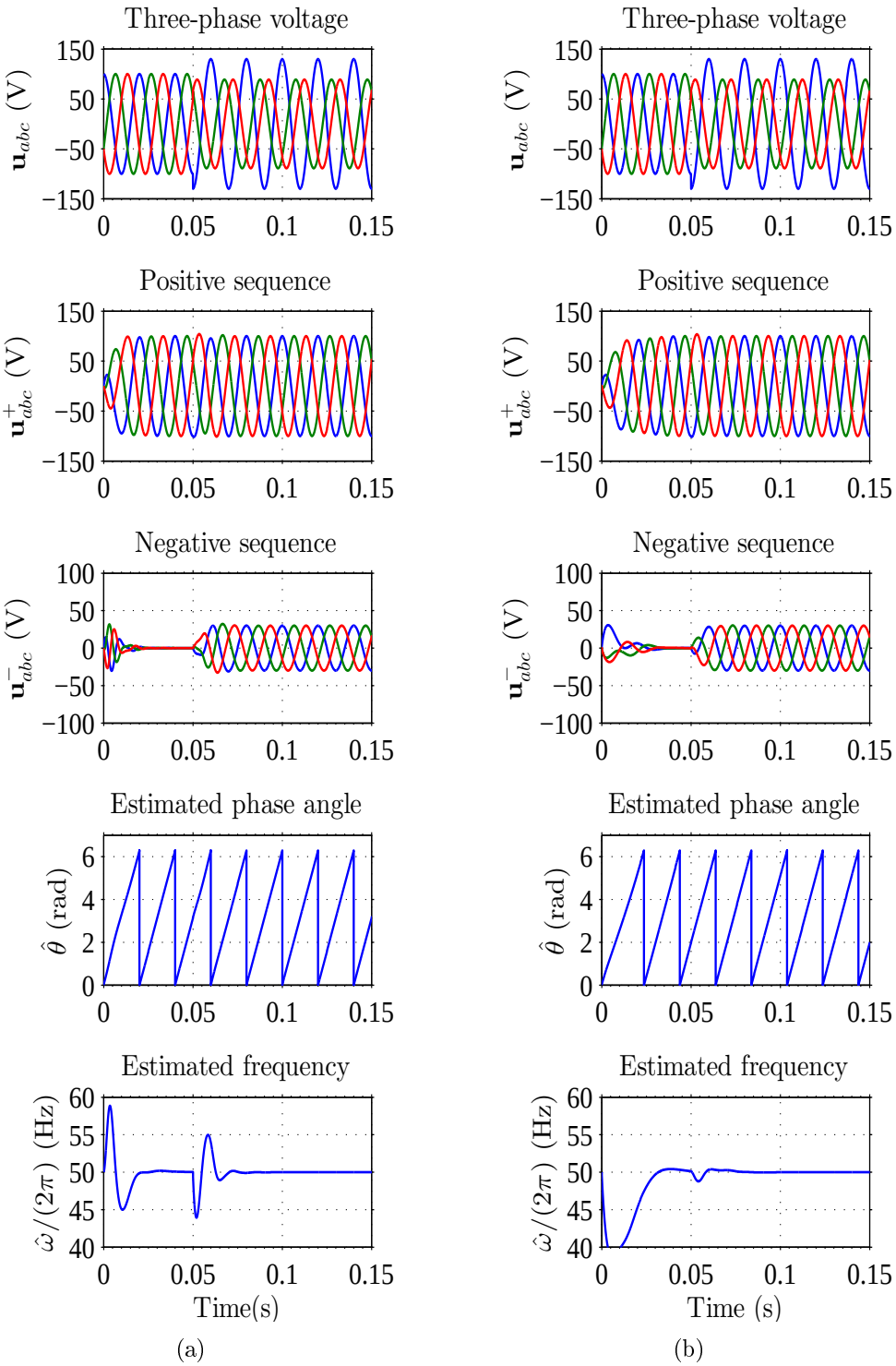

Figure 23: Performance of (a)DDSRF-PLL and (b) DSOGI-FLL under unbalanced condition. Unbalanced grid parameters: $U_+ = 100$ V, $U_- = 30$ V, $\omega = 50$ Hz.

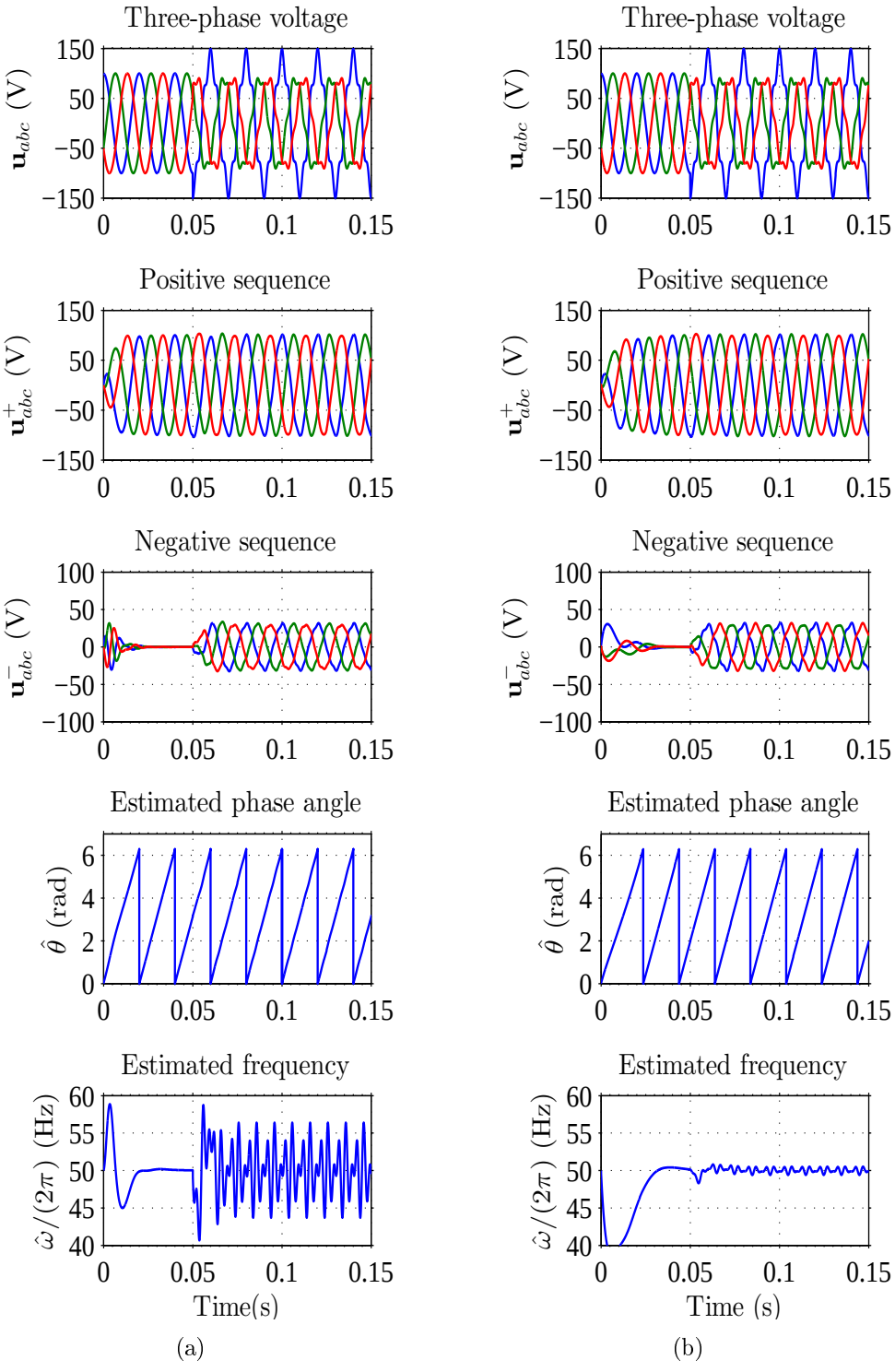

Figure 24: Performance of (a)DDSRF-PLL and (b) DSOGI-FLL under harmonic-distorted condition. Unbalanced grid parameters: $U_{+} = 100$ V, $U_{-} = 30$ V, $U_{+5} = 10$ V, $U_{-5} = 10$ V, $\omega = 50$ Hz.

8.3 Performance with Jumps in the Grid-voltage Amplitude and Frequency

DDSRF-PLL and DSOGI-FLL are tested with an unbalanced grid voltage, affected by jumps in the grid-voltage amplitude and frequency. In this case, the positive- and the negative-sequence voltage phasors of the grid voltage are $U_+ = 50$ V, $U_- = 25$ V, frequency changes from $\omega = 50$ Hz to $\omega = 45$ Hz under fault conditions, being the prefault grid voltage equal to $U_{\text{pf}} = 100$ V. The tuning parameters of the DSOGI-FLL are set to $k = \sqrt{2}$ and $\Gamma = 50$, as justified in Section 6. The control parameters for DDSFRF-PLL are selected as $K_p = 2.22$ and $k_i = 246.7$ to get $\omega_{\text{PLL}} \approx 2\pi 25$ rad/s and $\xi_{\text{PLL}} \approx 1/\sqrt{2}$. The unbalanced condition or fault appears after 0.05 s from balanced condition.

Fig. 25(a) shows the performance of DDSRF-PLL and Fig. 25(b) shows the performance of and DSOGI-FLL. The positive- and negative-sequence components estimated by the DDSRF-PLL are almost similar to the ones obtained with the DSOGI-FLL. The detection of the grid frequency in the DDSRF-PLL is not as good as the one achieved with the DSOGI-FLL. The DDSRF-PLL has a small overshoot in the estimated frequency. From the results presented in this example, it can be said that both DDSRF-PLL and DSOGI-FLL give almost similar result except the overshoot in the frequency estimation obtained with DDSRF-PLL.

8.4 Performance Under Voltage Sags and Phase Angle jump

Both DDSRF-PLL and DSOGI-FLL are simulated under all the classified voltage sags from A-G mentioned in section 2.3 with $D = 0.5\angle 0°$. The performance of both DDSRF-PLL and DSOGI-FLL are almost similar to each other in all the cases and they can accurately estimate the positive- and negative-sequence voltage, phase angle and frequency of the unbalanced systems.

It is said earlier in section 6, that FLL estimates the frequency of an input signal, which is not affected by sudden phase angle changes and might be advantageous then PLL based algorithms in that case. To verify this, a voltage sag type C with $D = 0.5\angle -30°$ is applied on DDSRF-PLL and DSOGI-FLL. In this case, the positive- and the negative-sequence voltage phasors of the grid voltage are $U_+ = 73\angle -9.9°$ V, $U_- = 25\angle 23.8°$ V, frequency $\omega = 50$ Hz, being the prefault grid voltage equal to $U_{\text{pf}} = 100$ V. The tuning parameters of the DSOGI-FLL are set to $k = \sqrt{2}$ and $\Gamma = 50$ and for DDSFRF-PLL are selected as $k_p = 2.22$ and $k_i = 246.7$ to get $\omega_{\text{PLL}} \approx 2\pi 25$ rad/s and $\xi_{\text{PLL}} \approx 1/\sqrt{2}$. The unbalanced condition or fault appears after 0.05 s from balanced condition.

Fig. 26(a) and 26(b) shows the performance of DDSRF-PLL and DSOGI-FLL, respectively. We can see that both DDSRF-PLL shows slow dynamics and oscillation for detecting the positive- and negative sequence voltage. DDSRF-PLL also cannot perfectly detect the phase angle of the positive sequence and as a result it

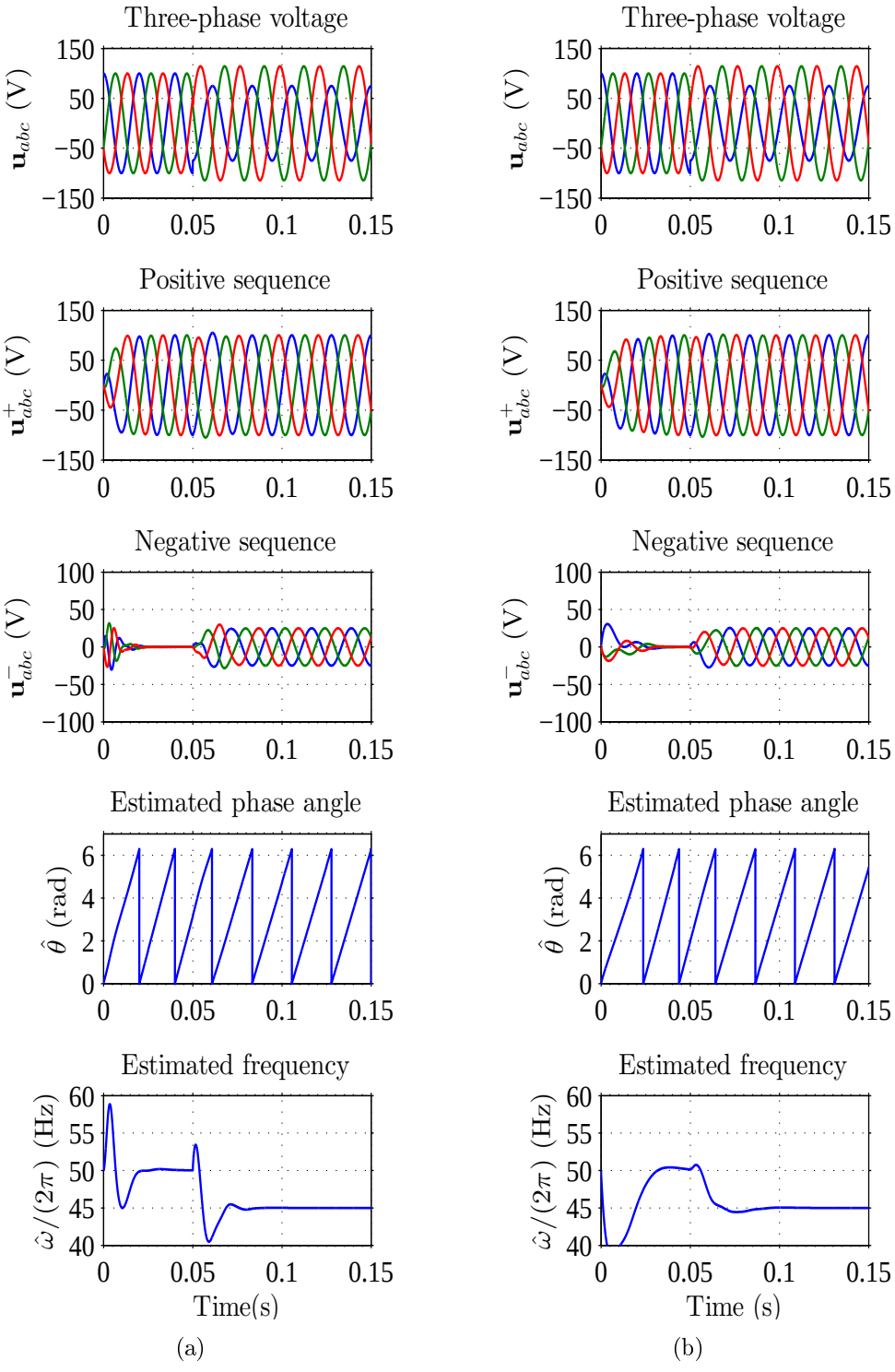

Figure 25: Performance of (a)DDSRF-PLL and (b) DSOGI-FLL with jumps in the grid-voltage amplitude and frequency. Unbalanced grid parameters: $U_{+} = 50$ V, $U_{-} = 25$ V, frequency changes from $\omega = 50$ Hz to $\omega = 45$ Hz.

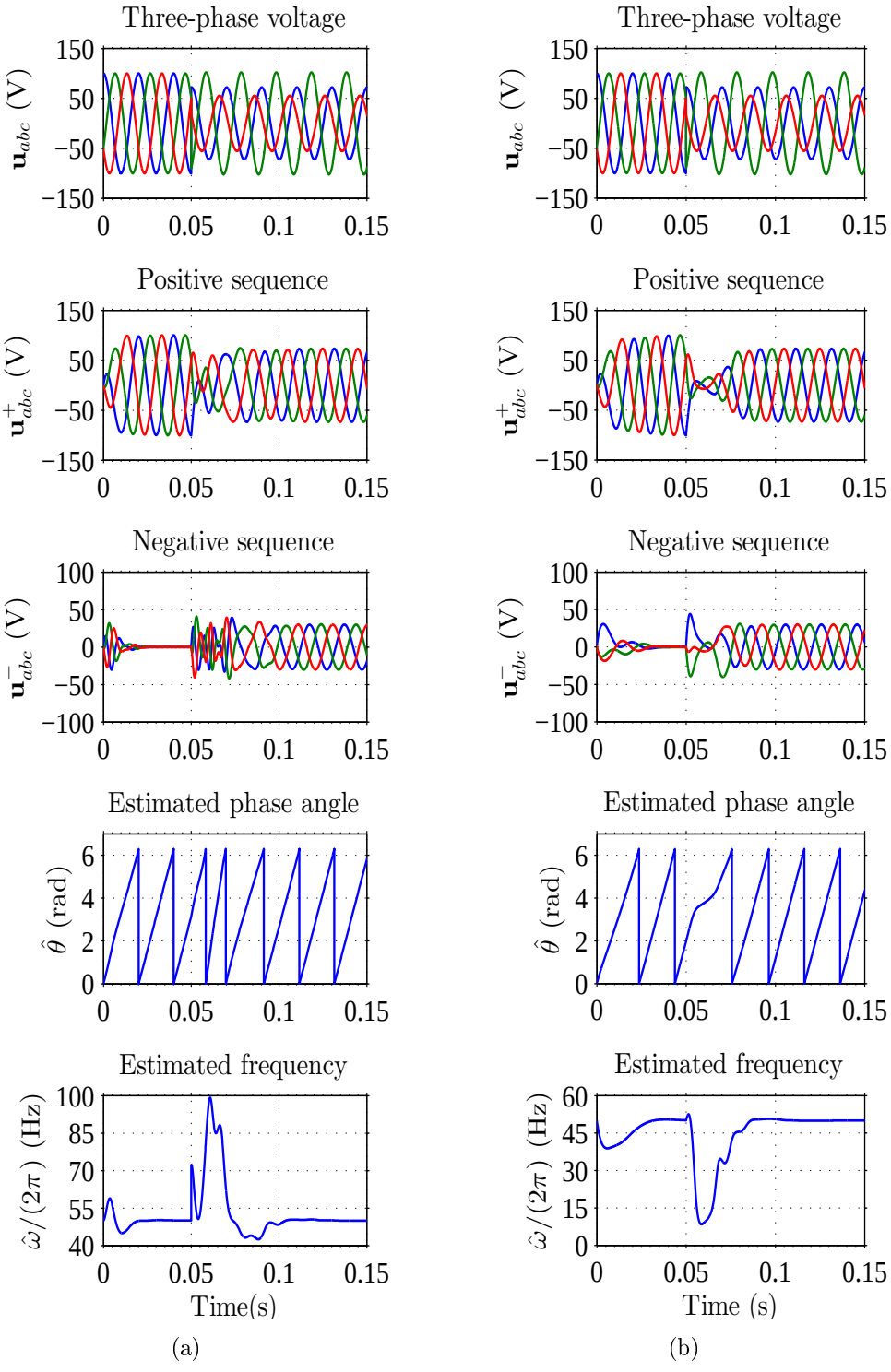

Figure 26: Performance of (a)DDSRF-PLL and (b) DSOGI-FLL under sag type C with $D = 0.5\angle{-30}°$. Unbalanced grid parameters: $U_{+} = 73\angle{-9.9}°$ V, $U_{-} = 25\angle{23.8}°$ V, frequency $\omega = 50$ Hz.

gives much more overshoot in the estimation of frequency. DSOGI-FLL also shows slow dynamics but less oscillation for detecting the positive- and negative sequence voltage. DSOGI-FLL can perfectly detect the phase angle of the positive sequence, but also shows some overshoot in the estimation of frequency. So, in the case of sudden phase angle jumps in the grid voltage, DSOGI-FLL shows better performance then DDSRF-PLL.

8.5 Performance of DDSRF-PLL with Control Loop Frequency 50 Hz

The value for the control loop frequency of DDSRF-PLL is selected as $\omega_{\text{PLL}} \approx 2\pi 25$ rad/s in previous examples. According to the modern grid codes, the strictest continuous operation limits for frequency appear in the British code is $47.5 - 52$ Hz and the most extreme frequency limits 46.5 Hz and 53.5 Hz are for E.ON offshore [35].

Now, to examine the performance of DDSRF-PLL with $\omega_{\text{PLL}} \approx 2\pi 50$ rad/s, which is same as grid frequency $\omega = 2\pi 50$ rad/s, the tuning parameters of the PLL are revised as $k_p = 4.44$ and $k_i = 986.96$ and simulated again for all the examples shown above. The performance is DDSRF-PLL is almost similar interms of estimating the value of positive- and negative-sequence voltage and the phase angle. But for estimating the frequency, there is higher overshoot in the case of $\omega_{\text{PLL}} \approx 2\pi 50$ rad/s than $\omega_{\text{PLL}} \approx 2\pi 25$ rad/s. As an example, an unbalanced harmonic distorted utility voltage is selected for examine as section 8.2. Fig. 27(a) and 27(b) shows the performance of DDSRF-PLL with $\omega_{\text{PLL}} \approx 2\pi 25$ rad/s and $\omega_{\text{PLL}} \approx 2\pi 50$ rad/s, respectively. As we can see that as the bandwidth of control loop is increased to be equal with the grid frequency, there is much more overshoot for estimating the frequency in Fig. 27(b) than 27(a).

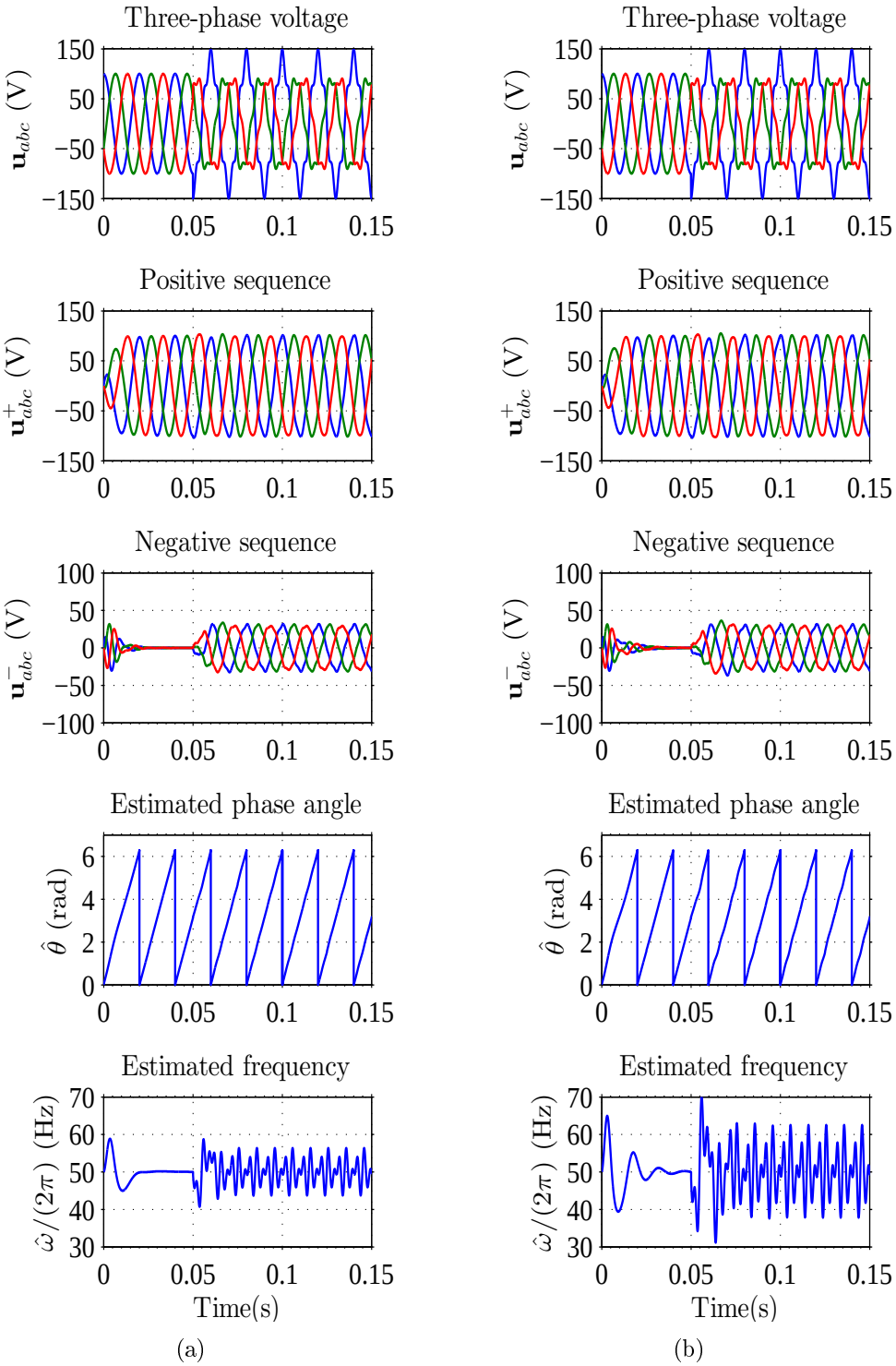

Figure 27: Performance of DDSRF-PLL under harmonic-distorted condition with (a) $\omega_{\text{PLL}} \approx 2\pi 25$ and (b) $\omega_{\text{PLL}} \approx 2\pi 50$. Unbalanced grid parameters: $U_{+} = 100$ V, $U_{-} = 30$ V, $U_{+5} = 10$ V, $U_{-5} = 10$ V.

9 Conclusion

In this thesis, two novel grid-voltage synchronization algorithms have been presented and compared with each other. After all the simulation results, the performance of DDSRF-PLL can be justified as below:

1. DDSRF-PLL can perfectly detect the positive- and negative-sequence component of the voltage by cancelling out the 2ω oscillation in the case voltage unbalanced condition.

2. The control loop bandwidth of DDSRF-PLL is selected as $\omega_{\mathrm{PLL}} \approx 2\pi 25$, which is half of the grid frequency of the input voltage. This might can be improved.

3. DDSRF-PLL cannot perfectly detect the positive- and negative voltage and frequency of the unbalanced voltage, when their is harmonic distortion in the input voltage. This is because DDSRF-PLL only cancels out the 2ω oscillation with the help of decoupling network. Meanwhile, it cannot cancels out the oscillation higher than 2ω. Which means if the amplitude of the harmonics is higher enough, it can cause much problem in the detection of positive- and negative sequence component of the voltage. A alternative solution for this might be the use of active and adaptive filtering [29]-[30] or multi-sequence/harmonic decoupling cell (MSHDC) [33] to cancel out the harmonic oscillations at any order automatically.

4. DDSRF-PLL also shows higher overshoot in the frequency estimation and slow dynamics comapred to DSOGI-FLL in the case of phase angle jump in the input unbalanced voltage.

The performance of DSOGI-FLL can be justified as below:

1. DSOGI-FLL can perfectly detect the positive- and negative-sequence component of the voltage by cancelling out the 2ω oscillation in the case voltage unbalanced condition.

2. DSOGI-FLL shows some oscillation in the detection of positive- and negative-sequence voltage and frequency, when their is harmonic distortion in the input voltage. This can be improved by means of using Multiple SOGI-FLL (MSOGI-FLL) [34] for cancelling the harmonic oscillation.

3. DSOGI-FLL shows higher overshoot in the frequency estimation, but faster dynamics comapred to DSOGI-FLL in the case of phase angle jump in the input unbalanced voltage.

4. DSOGI-FLL is implemented in stationary reference frame. But, when the control of the GSC is implemented in the synchronous reference frame, DSOGI-FLL is not the appropriate solution in that case.

9.1 Future Work

The grid synchronization algorithm MSHDC, which has mentioned earlier in this section, is implemented using $\alpha\beta$PLL [23]. The $\alpha\beta$PLL is implemented in stationary reference frame for estimation the phase angle of the positive-sequence voltage. The reason for the use of $\alpha\beta$PLL is that, it shows faster dynamics then SRF-PLL, as shown in [23]. But the use of $\alpha\beta$PLL might not be useful, when the control of the GSC is implemented in SRF.

A new algorithm based on SRF-PLL, decoupled multiple SRF-PLL (DMSRF-PLL) might be a better solution, when the utility voltage contains harmonic distortion. The idea of DMSRF-PLL is similar to DDSRF-PLL. The DDSRF-PLL can only remove the oscillation at 2ω. But it cannot remove the oscillations higher then 2ω, which are the results of decoupling of harmonics. DMSRF-PLL will have multiple decoupling cells having the ability of decoupling of the harmonics, which will cancel out the oscillations at any order resulted by the harmonic distortion. As a result, DMSRF-PLL will have the ability of perfectly detecting the positive and negative sequence components of the grid voltage. The control loop frequency and the grid frequency, both will be similar for DMSRF-PLL. Hence, there will be no need to reduce the bandwidth of the control loop, which will satisfy the modern grid codes [35].

I believe, that for both DDSRF-PLL and DSOGI-FLL, there are many more points to be improved, specially the performances under harmonic-distorted condition and phase angle jumps in the voltage at PCC. Otherwise, the performance of both DDSRF-PLL and DSOGI-PLL shows good dynamics response and appropriate FRT operation under grid faults in order to meet the modern grid codes.

References

[1] Teodorescu, R., Liserre, M. and Rodriguez, P. *Grid Converters for Photovoltaic and Wind Power Systems.* John Wiley and Sons, Inc., UK, 2011. ISBN 9780470057513.

[2] Blaabjerg, F., Teodrescu, R., Liserre, M., Timbus, A. *Overview of control and grid synchronization for distributed power generation systems.* IEEE Transactions on Industrial Electronics, vol. 53, no. 5, pp 1398-1409, October 2006.

[3] Abdalrahman, A., Zekry, A., Alshazly, A. *Simulation and Implementation of Grid-connected Inverters.* International Journal of Computer Applications (0975 - 8887), vol. 60, no.4, December 2012.

[4] Chung, S. *A phase Tracking System for Three phase Utility Interface Inverters.* IEEE Transactions on Power Electronics, vol. 53, no. 3, May 2000.

[5] Rodriguez, P., Bergas, J., Gallardo, J.A. *A new positive sequence Voltage Detector for Unbalanced Power System.* EPE-PEMC 2002 Dubrovnik and Cavat.

[6] Rodriguez, P., Sainz, L., Bergas, J. *Synchronous Double Reference Frame PLL applied to a Unified Power Quality Conditioner.* 10th International Conference on Harmonics and Quality of Power, vol.02, pp 614-619, October 2002.

[7] Freijedo, F., Doval-Gandoy, J., Lopez, O., Martinez-Penalver, C., Yepes, A., Fernandez-Comesana, P., Malvar, J., Nogueiras, A., Marcos, J. and Lago, *A. Grid-Synchronization Methods for Power Converters.* 35th Annual Conference of IEEE Industrial Electronics, pp. 522 - 529, November 2009.

[8] Rodriguez, P., Pou, J., Bergas, J., Candela, J., Burgos, R. and Boroyevich, D. *Decoupled double synchronous reference frame PLL for power converters control.* IEEE Transactions on Power Electronics, vol. 22, no. 2, pp. 584-592, 2007.

[9] Rodriguez, P., Luna, A., Munoz-Aguilar, A., Etxeberria-Otadui, I., Teodorescu, R. and Blaabjerg,, F. *A Stationary Reference Frame Grid Synchronization System for Three-phase Grid-connected Power Converters Under Adverse Grid Conditions.* IEEE Transactions on Power Electronics, vol. 27, no. 1, January 2012.

[10] Rodriguez, P., Luna, A., Ciobotaru, M., Teodorescu, R. and Blaabjerg,, F. *Advanced Grid Synchronization System for Power Converters under Unbalanced and Distorted Operating Conditions.* 32nd Annual Conference on IEEE Industrial Electronics, IECON 2006, pp. 5173-5178, November 2006.

[11] Rodriguez, P., Luna, A., Candela, I., Mujal, R., Teodorescu, R. and Blaabjerg, F. *Multiresonant Frequency-Locked Loop for Grid Synchronization of Power Converters Under Distorted Grid Conditions.* IEEE Transactions on Industrial Electronics, vol. 27, no. 1, pp. 127-138, January 2011.

[12] Widrow, B., Glover, Jr, J., McCool, J., Kaunitz, J., Willaims, R., Hearn, R., Zeidler, J., Dong, Jr. E., Goodlin. R. *Adaptive Noise Cancelling: Principles and Applications.* Proceedings of the IEEE, vol. 63, no. 12, pp. 1692-1716, December 1975.

[13] Glover, Jr, J. *Adaptive Noise Cancelling Applied to Sinusoidal Interferences.* IEEE Transactions on Acoustics, Speech and Signal Processing, vol. 25, pp. 484-491, December 1977.

[14] Yuan, X., Merk, W., Stemmler, H., Allmeling, J. *Stationary-Frame Generalized Integrators for Current Control of Active Power Filters With Zero Steady-State Error for Current Harmonics of Concern Under Unbalanced and Distorted Operating Conditions.* IEEE Industry Applications Conference, 2000 , vol. 4, pp. 2143-2150, October 2000.

[15] Teodorescu, R., Blaabjerg, F., Liserre, M., Loh, P.C. *Proportional-resonant controllers and filters for grid-connected voltage-source converters.* IEE Proceedings on Electric Power Applications, vol. 153, pp. 750-762, September 2006.

[16] Zmood, D.N., Holmes, D.G. *Stationary Frame Current Regulation of PWM Inverters With Zero Steady-State Error.* IEEE Transactions on Power Electronics, vol. 18, pp. 814-822, May 2003.

[17] Mojiri, M., Bakhshai, R. *An Adaptive Notch Filter for Frequency Estimation of a Periodic Signal.* IEEE Transactions on Automatic Control, vol. 49, pp. 314-318 , February 2004.

[18] Mojiri, M.,Karimi-Ghartemani, M., Bakhshai, A. *Estimation of Power System Frequency Using an Adaptive Notch Filter.* IEEE Transactions on Instrumentation and Measurement, vol. 56, pp. 2470-2477, December 2007.

[19] Rodriguez, P., Teodorescu, R., Candela, I., Timbus, A.V., Liserre, M. and Blaabjerg, F. *New Positive-sequence Voltage Detector for Grid Synchronization of Power Converters under Faulty Grid Conditions.* 37th IEEE Power Electronics Specialists Conference, 2006. PESC '06., pp. 1-7, June 2006.

[20] Ciobotaru, M., Teodorescu, R., Blaabjerg, F. *A New Single-Phase PLL Structure Based on Second Order Generalized Integrator.* 37th IEEE Power Electronics Specialists Conference, 2006. PESC '06., pp. 1-6, June 2006.

[21] Franklin, G., Powell, J., Emami-Naeini, A. *Feedback control of Dynamic Systems.* Englewood Cliffs, NJ: Prentice-Hall, 2009.

[22] Rodriguez, P., Luna, A., Teodorescu, R., Iov, F. and Blaabjerg, F. *Fault Ride-through Capability Implementation in Wind Turbine Converters Using a Decoupled Double Synchronous Reference Frame PLL.* European Conference on Power Electronics and Applications, 2007. pp. 1-10, September 2007.

[23] Hadjidemetriou, L., Kyriakides, E. and Blaabjerg, F. *A New hybrid PLL for Interconnecting Renewable energy Systems to the Grid.* IEEE Transactions on Industry Applications, vol. 49, no. 6, November/December 2013.

[24] Rodriguez, P., Pou, J., Candela, I., Burgos, R. and Boroyevich, D. *Double Synchronous Reference Frame PLL for Power Converters Control.* IEEE 36th Power Electronics Specialists Conference, 2005. pp. 1415-1421, June 2005.

[25] Rodriguez, P., Luna, A., Candela, I., Teodorescu, R. and Blaabjerg, F. *Grid Synchronization of Power Converters using Multiple Second Order Generalized Integrators.* in Proc. 34th Annu. Conf. IEEE Ind. Electron., pp. 755-760, Nov. 10-13, 2008.

[26] Lyon, W. *Application of the Method of Symmetrical Components.* New York: McGraw-Hill, 1937.

[27] Harnefors, L. *Control of Variable-speed Drives.* " Applied Signal Processing and Control, Department of Electronics, Mälardalen University " , Sweden, 2003.

[28] Gardner, F. *Phaselock Techniques.* John Wiley and Sons, Inc., USA, 1979. ISBN 0-471-04294-3.

[29] Carugati, I., Maestri, P., Donato, G., Carrica, D. and Benedetti, M. *Variable Sampling Period Filter PLL for Distorted Three-phase Systems.* IEEE Transactions on Power Electron., vol. 27, no. 1, pp. 321-330, Jan. 2012.

[30] Gonzalez-Espin, F., Garcera, G., Patrao, I., Figueres, E. and Benedetti, M. *An Adaptive Control System for Three-phase Photovoltaic Inverters Working in a Polluted and Variable Frequency Electric Grid.* IEEE Transactions on Power Electron., vol. 27, no. 10, pp. 4248-4261, Oct. 2012.

[31] Bollen, M. and Gu, I. *Signal Processing for Power Quality Disturbances.* Hoboken, NJ, USA: Wiley-IEEE Press, 2006, ch. 8.

[32] Bollen, M. *Understanding Power Quality Problems: Voltage Sags and Interruptions (Power Engineering Series).* Piscataway, NJ: IEEE Press, 2000.

[33] Hadjidemetriou, L., Kyriakides, E.and Blaabjerg, F. *Synchronization of Grid-connected Renewable Energy Sources Under Highly Distorted Voltages and Unbalanced Grid Faults.* 39th Annual Conference of the IEEE Industrial Electronics Society, IECON 2013, pp. 1887-1892, Nov. 10-13, 2013.

[34] Rodriguez, P., Luna, A., Candela, I., Teodorescu, R. and Blaabjerg, F. *Grid Synchronization of Power Converters using Multiple Second Order Generalized Integrators.* 34th Annual Conference of IEEE Industrial Electronics, IECON 2008, pp. 755-760, Nov. 10-13, 2008.

[35] Altin, M., Göksu, O., Teodorescu, R., Rodriguez, P., Jensen, B.-B. and Helle, L. *Overview of Recent Grid Codes for Wind Power Integration.* 12th International Conference on Optimization of Electrical and Electronic Equipment (OPTIM), 2010 , pp. 1152-1160, May. 20-22, 2010.